Fabric Development in a Middle Devonian Intraoceanic Subduction Regime: The Careón Ophiolite (Northwest Spain)
Author(s): J. Gómez Barreiro, J. R. Martínez Catalán, D. Prior, H.-R. Wenk, S. Vogel, F. Díaz García, R. Arenas, S. Sánchez Martínez, and I. Lonardelli
Reviewed work(s):
Source: *The Journal of Geology*, Vol. 118, No. 2 (March 2010), pp. 163-186
Published by: The University of Chicago Press
Stable URL: http://www.jstor.org/stable/10.1086/649816
Accessed: 10/12/2012 05:11

Fabric Development in a Middle Devonian Intraoceanic Subduction Regime: The Careón Ophiolite (Northwest Spain)

J. Gómez Barreiro, J. R. Martínez Catalán,[1] *D. Prior,*[2] *H.-R. Wenk,*[3] *S. Vogel,*[4] *F. Díaz García,*[5] *R. Arenas, S. Sánchez Martínez, and I. Lonardelli*[6]

Departamento de Petrología y Geoquímica–Instituto de Geología Económica CSIC, Universidad Complutense, 28040 Madrid, Spain
(e-mail: jugb@usal.es)

ABSTRACT

A Middle Devonian suprasubduction zone ophiolite, the Careón Unit (northwest Spain), displays amphibolite-facies ductile deformation fabrics related to the onset of the Rheic Ocean closure. Two different fabrics, an early high-*T* foliation and a subsequent lower-*T* foliation, each of which characterized by distinct deformation mechanisms, have been identified in two distinct crustal-scale shear zones of the same ophiolitic thrust sheet. Combined quantitative texture analysis by electron backscattered diffraction and time-of-flight neutron diffraction, were carried out on the shear zones and correlated with micro- and macrostructural data. The results indicate that the regional lineation and shear zone kinematics (east-west, top-to-the-east) represent fabrics developed essentially during the intraoceanic subduction of the Rheic Ocean, and their orientation may be considered a reference vector for convergence models in this part of the Variscan belt.

Introduction

Ophiolites provide unique information on the evolution of ancient arcs and oceans as well as the nature of collisional orogenesis (Nicolas 1989; Searle and Cox 1999; Dilek and Newcomb 2003; Beccaluva et al. 2004). In addition, ophiolites yield information on the structure and petrophysical properties of modern oceanic lithosphere and subduction systems (Ceuleneer et al. 1988; Vissers and Nicolas 1995; Parkinson and Pearce 1998; Godard et al. 2000; Boutelier et al. 2003), which determine the large-scale dynamics of the mantle-lithosphere system (Davies and Richard 1992; King 2001). Increasing evidence suggests that the distribution of ophiolites in time and space could be related to Earth-scale events such as superplumes (e.g., Vaughan and Scarrow 2003), supercontinent cycles (e.g., Worsley et al. 1984; Abbatte et al. 1985), and periods of major plate reorganization (e.g., Agard et al. 2007). Kinetic constraints are unfortunately restricted to oceanic lithosphere created during the last 180 m.yr. and to ophiolite complexes that have not undergone strong tectonization. Thus, information about plate convergence (e.g., relative motion, velocity, dynamic balance) retrieved from most of pre-Jurassic ophiolites is very limited and qualitative. On the other hand, the geodynamic significance of most ophiolites is well established, as the widespread occurrence of metamorphic soles (Nicolas 1989) and the distinct geochemical signature of immature arc (e.g., Pearce et al. 1984) point to an origin in an intraoceanic subduction zone (e.g., Jamieson 1986; Hacker 1994) for most ophiolites. The potential information preserved in ophiolites formed at the initial stages of convergence deserves our attention at different scales (e.g., Boudier et al. 1985, 1988; Aitchison et al. 2000; Beccaluva et al. 2004; Berly et al. 2006), as they

Manuscript received March 4, 2009; accepted October 19, 2009.

[1] Departamento de Geología, Universidad de Salamanca, 37008 Salamanca, Spain.
[2] Department of Earth Sciences, Liverpool University, Liverpool L69 3BX, United Kingdom.
[3] Department of Earth and Planetary Science, University of California, Berkeley, California 94720, U.S.A.
[4] Los Alamos Neutron Science Center, Los Alamos National Laboratory, Los Alamos, New Mexico 87545, U.S.A.
[5] Departamento de Geología, Universidad de Oviedo, 33005 Oviedo, Spain.
[6] Ingegneria dei Materiali e Tecnologie Industriali, Universitá degli studi di Trento,Trento I-38050, Italy.

[The Journal of Geology, 2010, volume 118, p. 163–186] 0022-1376/2010/11802-0004$15.00. DOI: 10.1086/649816

represent the ancient counterparts of modern intraoceanic subduction systems, whereas long-term evolution and deformation mechanisms within subducting and overriding plates are matters of debate (e.g., King 2001; Boutelier et al. 2003; Heuret and Lallemand 2005; Doglione et al. 2007; Heuret et al. 2007; Schellart et al. 2007; Schellart 2008).

Tracking the evolution of deformation fabrics in old ophiolites is not a trivial matter since we commonly deal with partially preserved sections, tectonically reorganized, with several stages of retrograde metamorphism (Hacker and Mosenfelder 1996; Díaz García et al. 1999). It has been shown that crystallographic-preferred orientation or texture analysis can provide independent and valuable evidence about the conditions of deformation and its kinematics. On that ground, quantitative characterization of textures in ophiolites may facilitate recognition of deformational stages, enable correlation of ophiolitic units, and complement petrological and geochemical studies. The study of olivine fabrics from mantle sections in ophiolites has provided important clues to the formation of oceanic mantle and deformation of the oceanic lithosphere (e.g., Ceuleneer et al. 1988; Nicolas et al. 1994; Michibayashi and Mainprice 2004). However, crustal sections of ophiolites, dominated by mafic rocks, typically have been ignored in quantitative fabric analyses, mainly because of their polymineral character, including low-symmetry phases (triclinic-monoclinic) as major components of the fabric, which result in complex diffraction patterns when conventional diffraction techniques are applied to analyze the preferred orientation of minerals (Siegesmund et al. 1994; Leiss et al. 2002; Pehl and Wenk 2005). The application of both time-of-flight (TOF) neutron diffraction and electron backscattered diffraction (EBSD) techniques (Prior et al. 1999; Xie et al. 2003; Wenk et al. 2003; Wenk 2006) and the Rietveld method for data refinement (Young 1993; McCusker et al. 1999) has successfully solved the fabric of complex crystalline materials (Xu et al. 2006; Gómez Barreiro et al. 2007*b*; Wenk et al. 2008).

In this article we investigate crystallographic-preferred orientation (or texture) in amphibolites from the crustal section of a suprasubduction zone ophiolite, the Careón Unit, one of the allochthonous terranes marking the suture of the Rheic Ocean in northwest Iberia. Structural and petrological features suggest that early intraoceanic subduction fabrics generated during the closure of the Rheic Ocean have been preserved in the ophiolite (Díaz García et al. 1999; Arenas et al. 2007*a*; Sánchez Martínez et al. 2007). Textural analyses on selected amphibolites from a high-temperature shear zone, corresponding to a metamorphic sole, and a mylonitic/ultramylonitic shear zone within one of the imbricate fault slices of the Careón ophiolite were carried out with TOF neutron diffraction and EBSD techniques to determine crystallographic-preferred orientation of the principal phases. The aim of our work is to improve our knowledge on the deformation history of the unit and to link it with the geodynamic frame of the closure of the Rheic Ocean.

Geological Context

Rheic (for Rhea, one of the Titans and sister of Iapetus in Greek mythology) is the name given to one of the oceanic realms closed during the Paleozoic convergence of Gondwana and Laurussia, preceding the assemblage of Pangea (Stampfli and Borel 2002; Murphy et al. 2006; Sánchez Martínez et al. 2007). It is accepted that the Rheic Ocean started opening between the Late Cambrian and Early Ordovician (Cocks and Torsvik 2002; Murphy et al. 2006; Arenas et al. 2007*a*, 2007*b*). Remnants of this ocean (in the form of ophiolites) and its continental margins have been identified in many parts of the Variscan-Appalachian belt, which was produced by the Laurussia-Gondwana collision (fig. 1). Most ophiolites commonly associated to the Rheic Ocean are Late Silurian to Early Devonian and show a distinct suprasubduction affinity (Sánchez Martínez et al. 2007). Evidence strongly suggest that old and dense lithosphere was consumed in an intraoceanic subduction zone.

Suprasubduction zone ophiolites crop out along the Variscan belt from the Iberian to the Bohemian massifs, including the Careón (northwest Iberia; Sánchez Martínez et al. 2007), Lizard (Cornwall; Nutman et al. 2001), Ślęża (Bohemian Massif; Dubińska et al. 2004) and, probably, Beja-Acebuches (southwest Iberia; Castro et al. 1996). These ophiolites are key elements to understanding the final stages of evolution of the Rheic Ocean as well as the early stages of convergence between Laurussia and Gondwana (Sánchez Martínez et al. 2007; Arenas et al. 2007*a*, 2007*b*; Martínez Catalán et al. 2009).

Two groups of ophiolites mark the Variscan suture in northwest Iberia (fig. 2) and represent two different stages in the evolution of the Rheic Ocean: the structurally lower ophiolitic units, of Cambro-Ordovician age, record the early evolution of the Rheic Ocean, whereas the upper ophiolitic

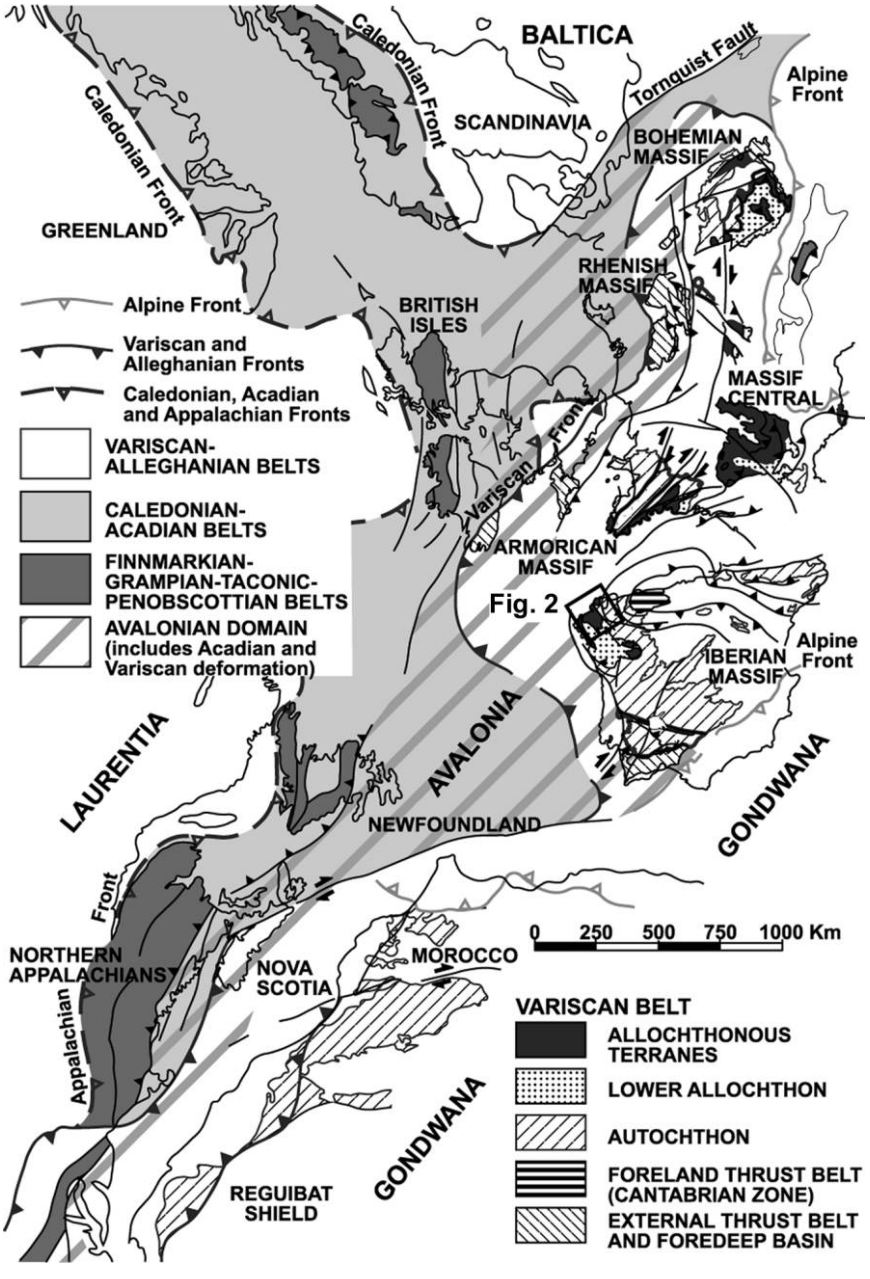

Figure 1. Location of Iberia in relation to the Paleozoic orogenic belts at the end of Variscan convergence. Location of figure 2 is indicated. Modified after Martínez Catalán et al. (2009) and Gómez Barreiro et al. (2007*a*).

units, Middle Devonian, preserve a record of the final stages in the evolution of the Rheic Ocean (Arenas et al. 2007*a*, 2007*b*). The lower ophiolitic units are represented by the Vila de Cruces Unit, which consists of an imbricate structure with variably deformed metapelitic schists, greenschists, felsic orthogneiss, metagabbro, and serpentinite. Regional foliation of pelitic schists, with high-*P*/low-*T* assemblages, have been dated at ca. 365 Ma ($^{40}Ar/^{39}Ar$, muscovite; Dallmeyer et al. 1997), while orthogneiss yielded an age of ca. 500 Ma (U-Pb, zircon; Arenas et al. 2007*b*).

The Careón Unit, which is the focus of this study, is one of the upper ophiolitic units. It consists of an imbricated stack (fig. 2) where crustal and mantle lithological associations of a suprasubduction

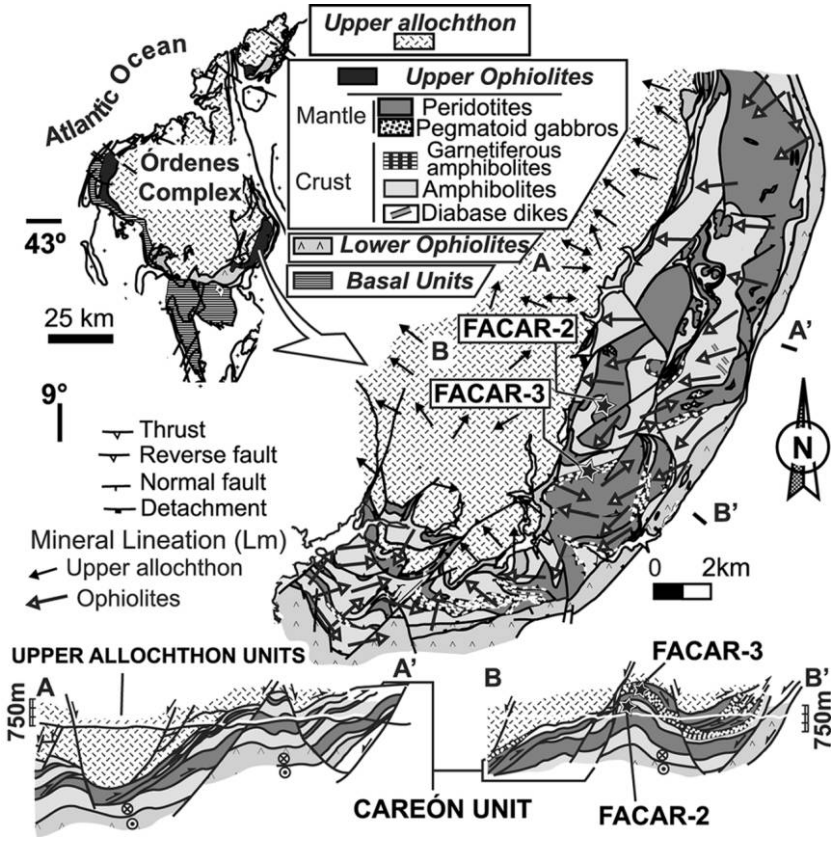

Figure 2. Geological map and representative cross sections of the Careón ophiolite and its location in the Iberian Massif (northwest Spain). The legend shows a summary of the allochthonous units in northwest Iberia. From top to bottom, upper allochthon, an arc-related terrane with a polyorogenic evolution; upper ophiolites, created in a suprasubduction environment during the closure of the Rheic Ocean; lower ophiolites, relics of the initial stages of the Rheic spreading; basal units, representing the outermost margin of northern Gondwana, subducted at the onset of the Variscan collision. Mineral lineations are indicated for the upper allochthon and the Careón Unit. Based on Díaz García et al. (1999), Gómez Barreiro et al. (2006), and Arenas et al. (2007*a*).

zone ophiolite are variably preserved between ductile shear zones. A complete transition from ultramafic rocks to isotropic metagabbros is found in tectonic sheets (Díaz García et al. 1999). Figure 3 summarizes structural and lithological relationships in one of these sheets. Shear zones, which bound structural sheets, recorded the main episode of deformation within the Careón Unit (fig. 3). This episode took place under conditions typical of the high-pressure and medium-to-high-temperatures part of the amphibolite facies (ca. 650° ± 55°C, 9.5 ± 1.5 kbar; Díaz García et al. 1999; Pin et al. 2002). Garnet- and corundum-bearing assemblages represent the maximum *P-T* conditions that were reached, and they are spatially linked to high-strain zones where a mylonitic fabric developed (figs. 3, 4). These structures are considered intraoceanic thrusts that led to the initial imbrication of the suprasubduction oceanic lithosphere and the formation of metamorphic soles during the closure of the Rheic Ocean (Díaz García et al. 1999; Sánchez Martínez et al. 2007). A retrograde stage followed, resulting in low-amphibolite to greenschist facies synkinematic mineral assemblages. These medium-temperature mylonitic amphibolites are volumetrically more common and occur in shear zones distributed throughout crustal sections of the Careón Unit (fig. 3). Semiquantitative estimations on these rocks support conditions below 650°C and 5 kbar (fig. 4) during this second stage (Pin et al. 2002).

Mantle sections of the Careón Unit consist of strongly serpentinized peridotites. Díaz García et al. (1999) interpreted scarce patches of recrystallized olivine in serpentinized peridotites as relics of a high-temperature fabric and correlated their

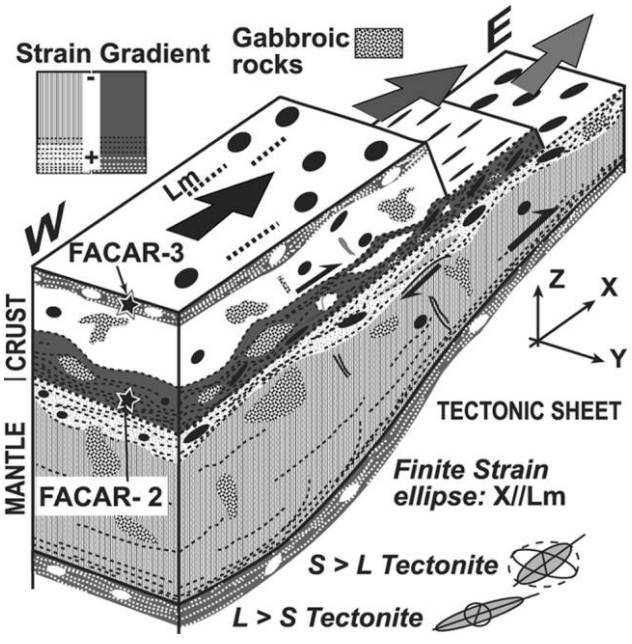

Figure 3. Idealized section (not to scale) of the middle tectonic sheet of the Careón ophiolite. Crustal and mantle portions are represented with different strain gradients. Main tectonic boundaries are thrust faults and/or high-grade shear zones. FACAR-3 type mylonites developed at high-temperature shear zones interpreted as metamorphic soles at top of the thrust sheets. High-strain zones developed throughout the whole crustal section and especially at the crust/mantle boundary (paleo-Moho), where FACAR-2 type mylonites were sampled. Finite strain ellipses are qualitative, derived from fabric inspection at the outcrop. Gabbroic rocks of different types intruded and resulted heterogeneously deformed elsewhere within the thrust sheet. The *XYZ* reference system is for texture analyses, with *X* parallel to the mineral lineation (Lm) and *XY* to the foliation. Solid arrows represent average orientation of Lm. The position of samples is indicated.

shape fabric (Lm; fig. 5) with fabrics preserved in the crustal section. The coincidence of shape and macro fabrics supports coherent deformation across the Careón Unit. However, since no textural data exist for the mantle section, partially due to the difficulty in finding well-preserved olivine-rich samples, it is necessary to be cautious when interpreting crust/mantle relationships.

Previous investigations established the origin and the metamorphic and structural evolution of the Careón unit as a whole (Díaz García et al. 1999; Sánchez Martínez et al. 2007). The mineral lineation in both crustal and mantle sections has a persistent east-west attitude (figs. 3, 5), and major, low-dipping shear zones related to thrust faults show kinematic criteria (σ-type porphyroclasts and S-C-C′ bands) with a dominant top-to-the-east movement, particularly in low-grade phyllonitic bands (Díaz García et al. 1999).

The gabbros in the Careón Unit yield protolith ages of ca. 395 Ma (U-Pb, zircon; Díaz García et al. 1999; Pin et al. 2002), whereas the regional tectonic foliation that was developed under amphibolite facies conditions yields $^{40}Ar/^{39}Ar$ ages between 390 and 376 Ma in this and other upper ophiolitic units (hornblende concentrates; Dallmeyer and Gil Ibarguchi 1990; Peucat et al. 1990; Dallmeyer et al. 1991, 1997). The amphibolite-facies fabric is related to ophiolite imbrication (Díaz García et al. 1999; Arenas et al. 2007*a*), and the narrow age interval between oceanic lithosphere generation and thrusting is consistent with a rapid deformation in a suprasubduction zone context.

Sample Description

Two metabasites located in the Careón ophiolite were sampled for texture analyses (figs. 2, 3). Both samples were collected from the same thrust sheet (Careón slice; Díaz García et al. 1999). (1) A garnet amphibolite (FACAR-3; figs. 2–4) that developed in a high-temperature shear zone (fig. 3) represents the

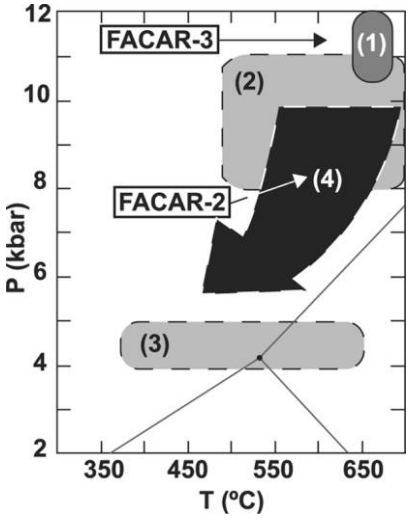

Figure 4. Pressure-temperature space for metabasites of the Careón ophiolite. Thermobarometric conditions as calculated for FACAR-3 type garnet-bearing amphibolites (Díaz García et al. 1999; *1*), hornblende-plagioclase assemblages in FACAR-2 type amphibolites (this work; Pin et al. 2002; *2*), retrograde conditions in FACAR-2 type amphibolites (this work; *3*); suggested *P-T* path for sample FACAR-2 (*4*). Aluminum silicate phase diagram after Holdaway (1971).

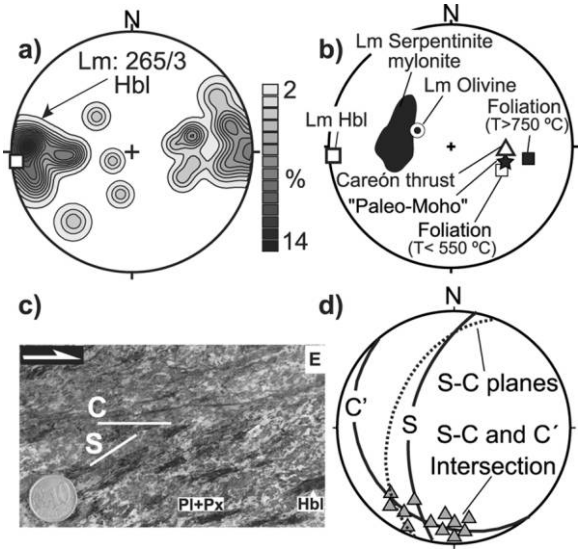

Figure 5. Structural analysis of the shape fabric of the Careón ophiolite. *a*, Stereographic projection of the mineral lineation in amphibolites across the unit, where a persistent east-west direction dominates over the effect of late folding (equal area, lower hemisphere projection, average mineral lineation (Lm) = 265°/3°). *b*, Compilation of structural data from Díaz García et al. (1999) and this study (equal angle stereographic projection, lower hemisphere). Note that the foliations defined by two different metamorphic assemblages ($T > 750$°C and $T <$ 550°C), the Careón thrust fault, and the paleo-Moho boundary are statistically indistinguishable, suggesting a continuous evolution. The lineations in the crustal and mantle sections also are coherent. *c*, Metagabbroic sample from the lower part of the Careón slice, where an S-C fabric shows a top-to-the-east shearing sense of movement (2-cm coin for scale). *S* = foliation, *C* = shear bands. *d*, Analysis of S-C-C′ structures. Intersections of S and C-C′ planes (*triangles*) are perpendicular to the flow direction (top-to-the-east or east-southeast). Hbl = hornblende, Pl = plagioclase, Px = pyroxene.

early stage of the mylonitic fabric as developed in an intraoceanic thrust (Díaz García et al. 1999). (2) A mylonitic amphibolite (FACAR-2; figs. 2–4) was collected in the inner part of the thrust sheet at the bottom of the crustal section, within a shear zone developed close to the contact between mafic and essentially ultramafic rocks, that is, the paleo-Moho (fig. 3). Sample FACAR-2 clearly represents the most deformed level within the crustal section as well as the most common type of mylonite in the Careón ophiolite.

Early High-Temperature Shear Zones: Sample FACAR-3. High-temperature garnet amphibolites are grano-nematoblastic, with a layered distribution of the main phases (fig. 6*b*). A pervasive tectonic fabric (S-L) dominates, with the lineation showing an east-west trend. A complete description of the mineral chemistry and microstructure can be found in Díaz García et al. (1999). According to these authors, the mineral assemblage is representative of peak metamorphic conditions and consists of Hbl + Pl + Grt + Ilm (mineral abbreviations after Kretz 1983). The amphibole can be described as hornblende with a medium to high content of Al_2O_3 (maximum 16.05%), Na_2O (maximum 2.32%), and TiO_2 (maximum 1.18%). No significant chemical zoning was detected in the amphiboles. Plagioclase is uniformly oligoclase in composition ($An_{23.57–18.78}$; maximum $Or_{0.54}$).

The sample is a banded amphibolite, with hornblende dominating the dark layers and showing irregular boundaries where small plagioclase grains commonly appear. Plagioclase grains are irregular, with lobate to partially straight contacts. Plagioclase aggregates may depict a mosaic texture that has been partially removed by grain-boundary migration. Ellipsoidal garnet poikioblasts can be recognized with quartz, and plagioclase inclusions. Local, low-grade microshears result in grain-size reduction by cataclastic flow and retrogression of primary minerals into quartz, epidote, and chlorite, and open voids and grain-boundary sliding features are commonly present.

P-T conditions of 10.5–12 kbar and 640°–680°C have been calculated from the mineral assemblage of the garnet-bearing amphibolites (Díaz García et al. 1999), providing an indication of the tectonic setting during which imbrication of the ophiolitic slices took place.

Inner Shear Zones: Sample FACAR-2. Nematoblastic amphibolites, with Hbl + Pl + Ep + Ttn ± Ilm ± Qtz ± Grt and a strong L-S tectonic shape fabric, represent the regional foliation and show an east-west to southeast-northwest mineral lineation defined mainly by amphiboles (figs. 2, 5). Kinematic criteria include asymmetric porphyroblasts and S-C bands with a coherent top-to-the-east sense of shear (fig. 6*a*). The microstructure ranges from mylonitic mixtures of Hbl and Pl with a load-bearing framework, to an interconnected distribution of weak layers (Handy 1994), depending on the amphibole to feldspar ratio. A banded microstructure is locally developed.

The sample (fig. 6*a*) has a mylonitic foliation with rounded plagioclase porphyroclasts with asymmetric recrystallization tails that indicate a top-to-the-east movement. Amphibole-rich bands with brown-green hornblende occur, whereas hornblende-plagioclase mixtures and lens-shaped, in-

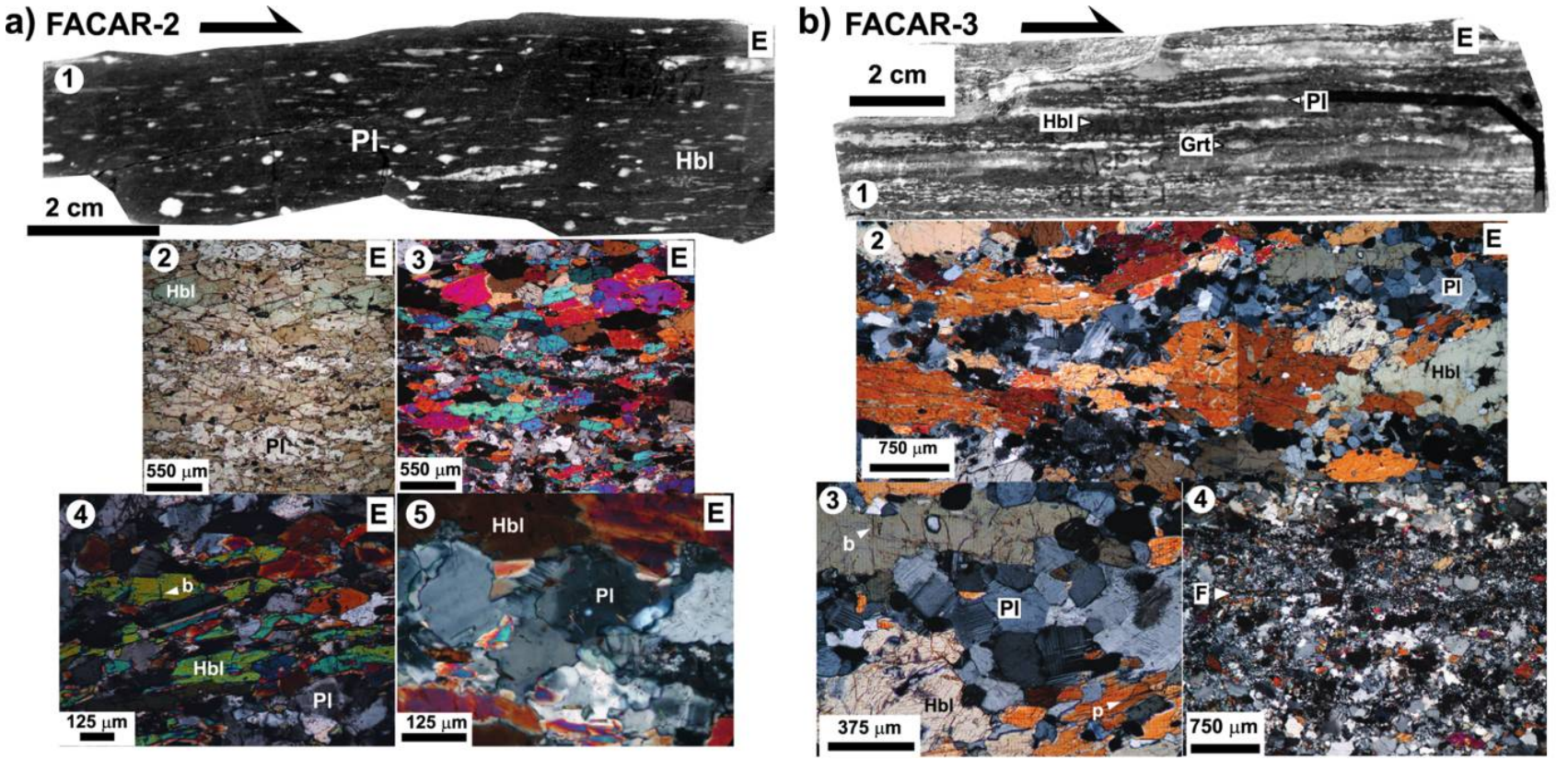

Figure 6. *a*, Fabric of FACAR-2 amphibolite. *1*, Mylonitic foliation with rounded plagioclase (*Pl*) porphyroclasts on which asymmetric recrystallization tails indicate a top-to-the-east movement. *Hbl* = hornblende. *2*, *3* (parallel/crossed-nicols), Petrographic detail of the FACAR-2 foliation. Amphibole-rich bands with brown-green hornblende, showing clear contacts and microcracks. Undulose extinction rarely developed in hornblende. Plagioclase with lobate shapes and twins shows undulose extinction. Ilmenite, titanite, and epidote are often present. *4*, Some hornblende microstructures: twins and basal microcracks (*b*). *5*, Detail of plagioclase aggregates, depicting irregular grain boundaries and chemical zoning. *b*, Overview of FACAR-3 amphibolite. *1*, Fabric with segregation of mineral phases in bands. Ellipsoidal garnets (*Grt*) are recognized. *2*, Composite microphotograph, showing representative bands of hornblende and plagioclase. Hornblende shows irregular boundaries where plagioclase often nucleates. Undulose extinction, basal and prismatic microcracks are also visible. Plagioclase grains are irregular, with lobate to partially straight contacts. Undulose extinction, twins and subgrains are present. *3*, Detail of plagioclase aggregate, with a mosaic texture partially removed by grain-boundary migration. Subgrains are also visible in some crystals. *p* = prismatic microcrack. *4*, Microshear planes (fault plane *F*) affecting a plagioclase layer with mosaic texture (*top*). Damage zones around fault plane result in grain-size reduction by cataclastic flow and retrogression of primary minerals into quartz, epidote, and chlorite. Open voids and grain-boundary sliding microstructures are often present along the contacts.

Table 1. Selected Microprobe Analyses of FACAR-2 Type Amphibolites

	Ca-amphibole[a,b]			Plagioclase		
	1 c	2 m	3 r	1 c	2 m	3 r
SiO_2	45.20	46.86	55.04	57.97	58.17	61.62
TiO_2	.48	.64	.14	.01	.01	.01
Al_2O_3	14.34	12.07	3.64	26.80	26.50	24.01
MnO	.22	.21	.17	.00	.01	.00
FeO[c]	11.33	11.25	9.28	.03	.08	.08
MgO	12.65	13.05	17.22	.00	.00	.00
CaO	11.37	11.51	12.18	7.81	7.56	4.69
K_2O	.23	.20	.05	.02	.02	.06
Na_2O	2.52	2.39	.83	7.20	7.38	8.94
F	.04	.03	.01			
Cl	.00	.00	.00	.00	.00	.01
Total	98.38	98.20	98.54	99.85	99.73	99.42
Si	6.46	6.72	7.69	2.60	2.61	2.75
AlIV	1.54	1.28	.31			
AlVI	.87	.76	.29			
Al	2.41	2.04	.60	1.41	1.40	1.26
Ti	.05	.07	.02	.00	.00	.00
Fe^{3+}	.35	.14	.10	.00	.00	.00
Fe^{2+}	1.01	1.21	.98			
Mn	.03	.03	.02	.00	.00	.00
Mg	2.70	2.79	3.59	.00	.00	.00
Ca	1.74	1.77	1.82	.37	.36	.22
Na	.70	.66	.23	.63	.64	.77
K	.04	.04	.01	.00	.00	.00
Mg/(Fe+Mg)	.73	.70	.79			
NaM4	.26	.23	.18			
Na(A)	.44	.43	.05			
K(A)	.04	.04	.01			
Σ cations	15.48	15.47	15.06	5.01	5.01	5.01
An				37.44	36.11	22.41
Ab				62.45	63.76	77.27
Or				.11	.13	.32

Note. r = rim; m = inner zones; c = core.
[a] Cations per 23 oxygens, normalized to 13 cations excluded Ca, Na, and K.
[b] Cations per 8 oxygens.
[c] Total iron as FeO.

terconnected plagioclase domains are common. A shape-preferred orientation (SPO) is parallel to the foliation. Ilmenite, titanite, and epidote are typically present.

Methodology

Microprobe Analysis. Chemical analyses were done for sample FACAR-2 (table 1) with a CAMECA SX51 electron probe at the Department of Earth and Planetary Science at the University of Califonia, Berkeley. Operating conditions were 15 kV, 30 nA. Data were reduced with ZAF corrections with software written by J. Donovan (Advanced Microbeam). Mineral analysis, analytical methods, and thermobarometry for sample FACAR-3 are given in Díaz García et al. (1999).

Microstructural Analysis. Observations were carried out in both samples with petrographic and electron microscopes on thin sections prepared parallel to the lineation and orthogonal to the foliation (*XZ* plane; fig. 7). Sections were chemically polished (Prior et al. 1996) and left uncoated. Manually digitized micrographs were analyzed with ImageJ, version 1.38 software (W. S. Rasband, U.S. National Institutes of Health, http://rsb.info.nih.gov/ij/, 1997–2006) and SPO 2003, version 6 (January 2008) software (Launeau and Robin 1996; http://www.sciences.univ-nantes.fr/geol/UMR6112/SPO). The grain size (d) is defined as the diameter of the equivalent circle with the same area (A) as the measured grain ($d^2 = 4A/\pi$; Heilbronner and Bruhn 1998). The shape ratio (SR) and the long-axis orientation of each grain (α) are calculated from the inertia tensor of its shape (Jähne 1991). The SR/α graphs were constructed from those data (fig. 8). Bulk SPOs (SRt, Φ) were calculated by averaging the inertia tensor of each grain, resulting in an SPO weighted by the area of each grain (Launeau and Cruden 1998). Bulk SPOs were used to correlate different aggregates and the relative contribution of each mineral phase to the rock fabric. Microcrack orientation distribution was calculated in hornblende in order to evaluate the effect of cataclasis and rigid rotation of grains into the fabric (Nyman et al. 1992; Shelley 1994; Imon et al. 2004).

Texture Analysis. *EBSD.* Both samples were analyzed to obtain the full crystallographic orientation data of mineral phases. Amphibole and garnet were obtained from automatically indexed EBSD patterns collected in a CamScan X500 crystal probe fitted with a thermionic field emission gun and a FASTRACK stage (Prior et al. 1999). We used an accelerating voltage of 20 kV, a beam current of 5nA, and a working distance of 26 mm (Prior et al.

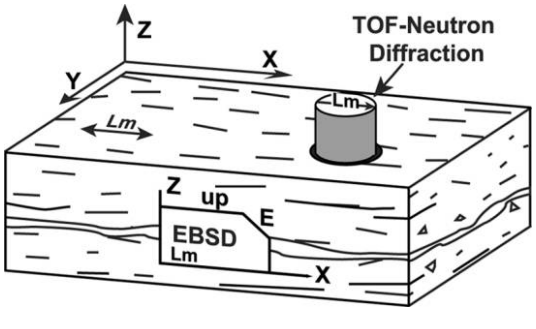

Figure 7. Reference system for texture analysis on electron backscattered diffraction (EBSD; thin section) and neutron diffraction (cylinder; TOF = time of flight). Lm = mineral lineation.

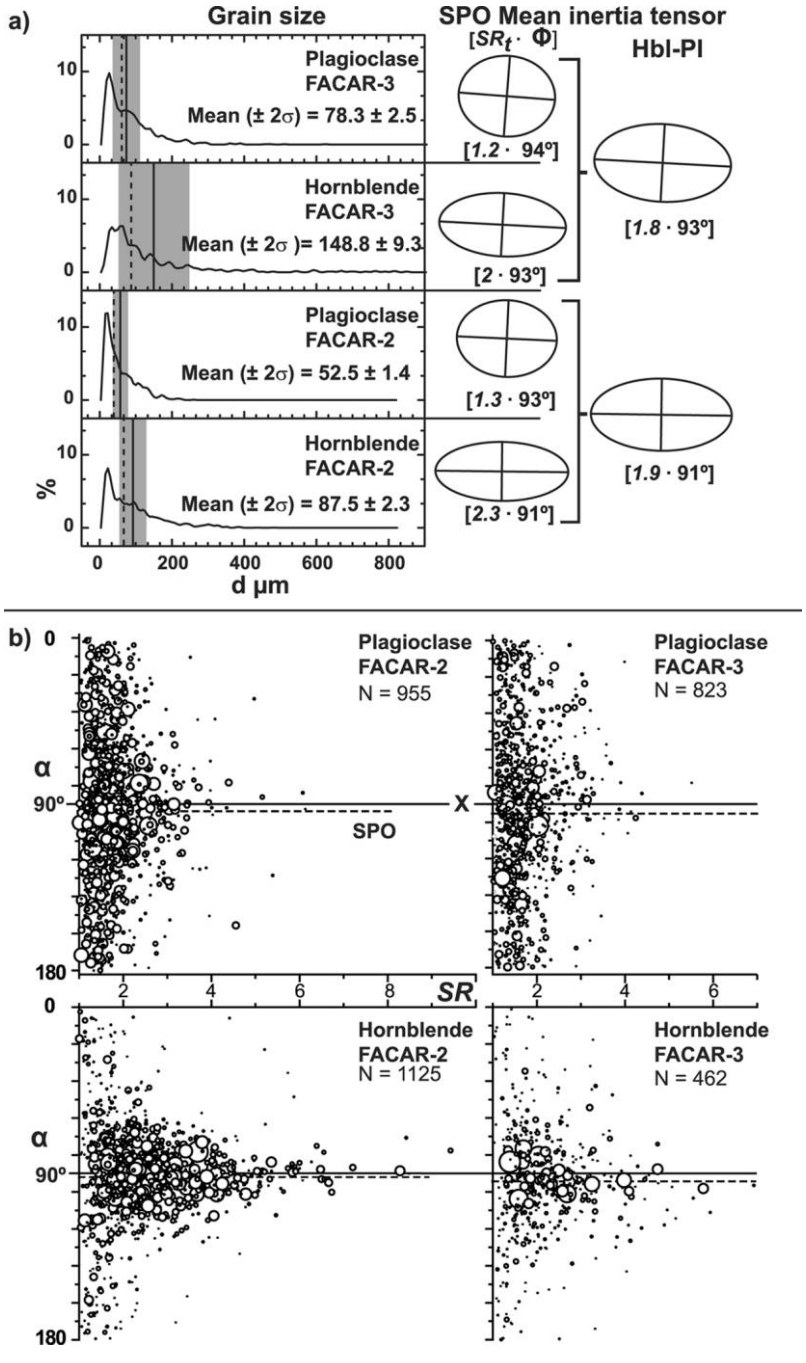

Figure 8. Microstructural data of the two samples analyzed. *a*, Grain-size distribution (*d*) for hornblende (Hbl) and plagioclase (Pl) in samples FACAR-2 and FACAR-3. Curves approximate to a lognormal distribution. Mean (*continuous line*), median (*dashed line*), and data dispersion (*gray area* = standard deviation, 2σ) are included. Average grain size is larger in sample FACAR-3 and hornblende. Shape-preferred orientation (SPO) and mean inertia tensor (Launeau and Robin 1996) are calculated for Hbl-Pl aggregates and minerals. Plagioclase displays a weak SPO and shape ratio (*SR*), while hornblende shows a strong SPO and SR. However, bimineral aggregates result in equivalent values. *b*, *SR*/α graphs, where the size of circles is proportional to *d*. A direct dependence of SR, long-axis orientation of each grain (α), and grain-size *d* arises in both samples for hornblende, while plagioclase has no significant preferred orientation nor evident grain-size dependency with SPO.

1996; Prior and Wheeler 1999). The EBSD patterns were indexed using the program Channel 5 (HKL Technology) and plotting crystallographic directions in pole figures in terms of Euler angles. Raw data were processed to provide a more complete reconstruction of the microstructure and to remove erroneous data on the basis of orientation maps (Prior et al. 1999). In all cases the selected area corresponds to mainly monomineralic bands of amphibole in order to optimize the acquisition processes.

The EBSD patterns of plagioclase were manually analyzed with a 20-kV accelerating voltage and a beam current of 3 nA, working at a distance of 25 mm (Prior and Wheeler 1999). Diffraction patterns from each plagioclase grain were indexed using the program Channel+ (Schmidt and Olesen 1989) and a reflector database for albite (Prior and Wheeler 1999). Since positive and negative forms can be distinguished in triclinic minerals, upper and lower hemisphere pole figures were used.

TOF Neutron Diffraction. An experiment was done in the neutron TOF diffractometer HIPPO (high-pressure-preferred orientation) at the Los Alamos Neutron Science Center (e.g., Xie et al. 2003; Gómez Barreiro et al. 2007*a*). Sample FACAR-3 was not considered for neutron diffraction because of the difficulties associated with local heterogeneities within the fabric (fig. 6*b*). An oriented cylinder of sample FACAR-2, 10 mm in length and 8 mm in diameter, was fully immersed in the neutron beam, resulting in better statistics than those from the EBSD method. For each measurement, the sample was rotated around the cylinder axis (perpendicular to the incident neutron beam) into four positions (0°, 45°, 67.5°, 90°) to improve pole figures angular coverage. At each position, data were collected for 30 min, resulting in a total exposure time of 120 min. TOF diffraction spectra (fig. 9) were analyzed with the Rietveld method as implemented in the software MAUD (material analysis using diffraction; Lutterotti et al. 1999). The orientation distribution (OD) resolution was 15°. The OD was exported from MAUD and then used in BEARTEX to calculate and plot pole figures (Wenk et al. 1998). In the Rietveld refinement, crystallographic structures (CIF files) were required. For monocline phases, the first setting has to be used, in both MAUD and BEARTEX (Matthies and Wenk 2009), which requires some transformations. For representations in this article we use labels for second setting (i.e., [010] is the 2-fold axis). It should be noted that due to the low crystal symmetry of major components, for example, hornblende (monoclinic) and plagioclase (triclinic), [100] [010] and [001] directions do not correspond to the pole of the respective crystallographic plane (100) (010) (001), except for [010] in the monoclinic system. Poles of (20–1) (010) (−102) and (−401) (010) (−104) were used as the best approximation to [100] [010] and [001] directions for plagioclase and amphibole, respectively (Xie et al. 2003; Gómez Barreiro et al. 2007*a*). In the case of epidote and titanite, poles to (201), (010), and (102) were used. When considering mineral composition and diffraction data, we used magnesio-hornblende (C/2m; Oberti et al. 1995), epidote (P21/m; Gabe et al. 1973), titanite (P21/a; Speer and Gibbs 1976), and andesine (P-1; Fitz Gerald et al. 1986) structures as the starting point for Rietveld analysis. Mineral overgrowths such as oligoclase in plagioclase are expected to have the same preferred orientation as andesine cores (e.g., Němec 1967), such that a common structure was considered. The texture refinement of minor phases

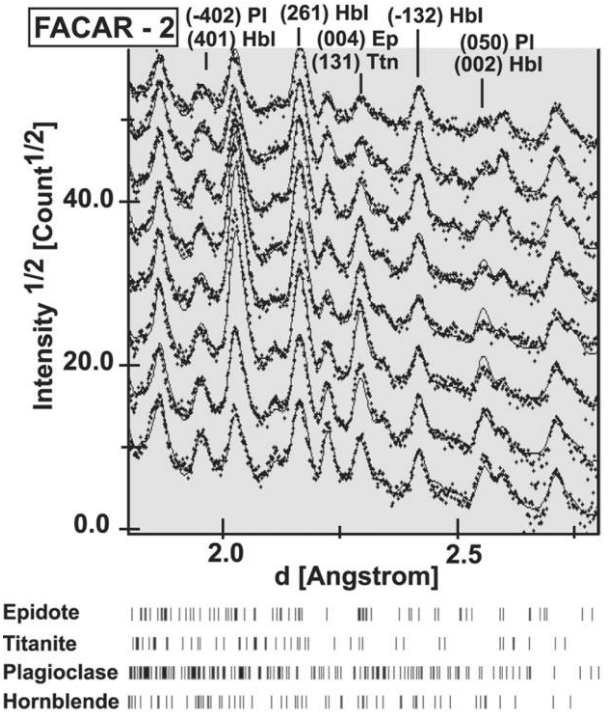

Figure 9. Example of diffraction spectra for amphibolite FACAR-2, recorded in HIPPO neutron diffractometer (150° bank). Relative intensity variations illustrate the presence of texture. Some important peaks are indexed. Dots represent measured data, and solid lines are the results of Rietveld refinement. Peak position for each mineral phase appears at the bottom illustrating the strong overlapping.

(<2% vol), like quartz and ilmenite, is below the resolution of the technique.

Results

Mineral Chemistry and Metamorphic Conditions. Selected microprobe analyses of amphibole and plagioclase from sample FACAR-2 are shown in table 1. Very small and rare garnet relics are not suitable for microprobe analysis. Saussuritic aggregates heterogeneously replace plagioclase and represent the latest retrograde stage.

The structural formulas for amphiboles were calculated by assuming total cations equalled 13 (except Ca, Na, and K; Leake 1978; Spear and Kimball 1984; Leake et al. 2004; Yavuz 2007). The characteristic amphibole is calcic amphibole, which can be classified in a broad sense as hornblende (table 1). Chemical variation across the crystals was detected, with tschermakitic/pargasitic cores, an inner zone that correspond to magnesio-hornblende, and an actinolitic rim that truncates the inner zones and appears asymmetrically distributed in the crystal (fig. 9*a*). These amphiboles exhibit a medium to high content in Al_2O_3 (maximum 14.50%), Na_2O (maximum 2.73%), and TiO_2 (maximum 0.89%).

The analyzed plagioclases show chemical zoning (fig. 10*b*; table 1). Two zones can be identified: (1) core and inner sectors correspond to andesine with an anorthite content ranging from 37.6 to 34.0 mol% and very low content of orthoclase (< 0.13 mol%). (2) Rim sectors are oligoclase (An23.6-An20.1; Or < 0.9), with a preferred development in orientations parallel to the foliation (fig. 11). We applied semiquantitative pressure indicators like the Al content in hornblende (e.g., Schmidt 1992; Anderson and Smith 1995) and the hornblende-plagioclase thermometer of Holland and Blundy (1994) to constrain *P-T* conditions. Results suggest *P-T* ranges of 7 ± 2 kbar and 650°–450°C.

Mineral relationships correlate with previous *P-T* estimations and interpretations (Díaz García et al. 1999; Pin et al. 2002), where the synkinematic growth of epidote, actinolitic hornblende rims, and oligoclase rims is linked to lower amphibolite facies assemblages (fig. 4).

Microstructures. The two analyzed samples have significant differences in microstructure. Grain-size distributions in both samples can be approximated by lognormal curves, skewed to the smallest sizes (fig. 8). Early high-*T* shear zones developed at metamorphic soles (FACAR-3) show a conspicuous banded distribution of phases, with a larger mean grain size (d) and a wider size distribution (2σ) than in mineral phases in shear zones developed later inside the tectonic sheets (FACAR-2; figs. 6, 8). Grains are different in shape. Amphibole in FACAR-3 has irregular boundaries with small and new grains of amphibole and plagioclase, while FACAR-2 (late inner shear zones) grains present much clearer and straighter boundaries. Plagioclase appears xenomorphic, with interlobate aggregates in both samples; however, in sample FACAR-3, polygonal shapes are locally identified (fig. 6*b*). Twins, undulose extinction, and subgrains in plagioclase are common in both samples, but they are only rarely developed in amphiboles. In sample FACAR-

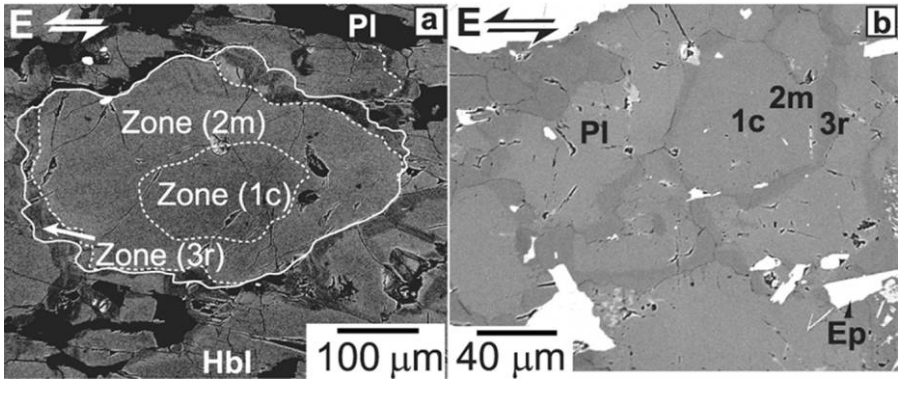

Figure 10. Example of chemical zoning in minerals from sample FACAR-2 (see table 1). *a*, Amphibole-rich band with pargasitic/magnesio-hornblende (*Hbl*; *1c-2m*) and actinolitic hornblende (*3r*) zones; *Pl* = plagioclase. *b*, Plagioclase-rich band, with andesine (*1c-2m*) and oligoclase (*3r*) zones. Chemical zoning appears frequently truncated and asymmetrically distributed (SEM micrographs, backscattered electron mode). Reference system as in figure 4 (section is *XZ* plane). *Ep* = epidote.

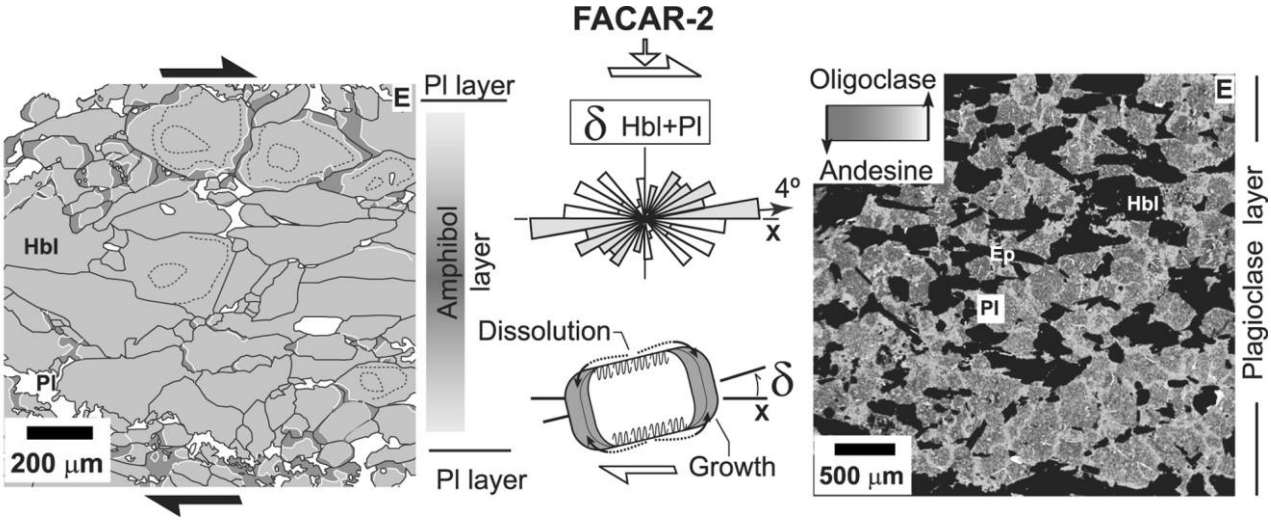

Figure 11. Analysis of crescent zones in hornblende (*Hbl*; *left*) and plagioclase (*Pl*; *right*) from FACAR-2. The δ is defined as the angle between the foliation plane and the pole to the long dimension of the crescent zone. Values are plotted together in a rose diagram where a slightly asymmetric distribution arises ($\delta = 4°$) coherent with the sense of shearing. However a stretching component seems to dominate the distribution, where boundaries with a pole close to the lineation experience statistically preferential growth. These features are compatible with stress-controlled solution transfer processes. *Ep* = epidote.

3, subgrain boundaries developed locally in amphibole, but such boundaries are rare in FACAR-2.

Plagioclase and amphibole mean SR is slightly higher in FACAR-2, but grain orientation (Φ) is similar. However, note that the average mean SR and grain orientation for the whole rock (Hbl-Pl aggregate) are indistinguishable for both samples. The SR/α graph reveals a different behavior of the principal phases (fig. 8). In both samples, the contribution of the plagioclase to the bulk SPO is low, and plagioclase grain orientation (α) shows a weak or null dependence on SR (fig. 8). Hornblende, however, displays a strong SR to α correlation: the higher the SR, the lower the variance of α, so the more intense the SPO. A direct correlation between grain size and SPO intensity is evident in hornblende, where larger grains display higher SR values and tend to align with α maximum (fig. 8). Bulk SPO is controlled by the hornblende fabric.

Preferred development of chemical zoning in plagioclase and amphibole from FACAR-2 was explored in backscattered images (fig. 11). Chemical zoning of hornblende and plagioclase occurs only in minerals from FACAR-2 and preferentially along plagioclase-rich layers adjacent to the boundary of hornblende-plagioclase layers (fig. 11). Truncated rims and crescent-shaped zones with a distinct chemical composition (table 1, 3 r) show a preferred distribution in the crystals (fig. 10). The orientation of those overgrowths with respect to the kinematic frame (*XYZ*) was analyzed along two quasi-monomineralic bands. A rose diagram of δ for amphibole and plagioclase is shown in figure 11, where δ is the subtended angle between the foliation and the pole to the crescent-shaped zones as defined in figure 11. Data from both minerals were plotted together since no significant differences exist. Although δ distribution is slightly asymmetric and synthetic with respect to shearing, the mean δ orientation ($\delta = 4°$) suggests that those faces perpendicular to the lineation preferentially developed overgrowths (fig. 11). Chemical evolution (table 1), suggests that the overgrowths developed during retrograde conditions.

Crystal microcracks mostly affect hornblende in both samples (fig. 6). Crack traces parallel to or at a small angle (<20°) to the [001] direction were grouped as prismatic (*p*, fig. 12), while those at a higher angles to the [001] direction were termed basal microcracks (*b*, fig. 12). Crack density was estimated, after pixel-size calibration, by comparing crack-to-grain total surface per sample. Crack density in FACAR-2 is double that of FACAR-3 amphiboles (fig. 12), with basal and prismatic microcracks respectively prevailing in FACAR-2 and -3. There is no evidence that microcracks induced relevant changes in the crystallographic orientation. Most of them do not cross the Hbl-Pl grain bound-

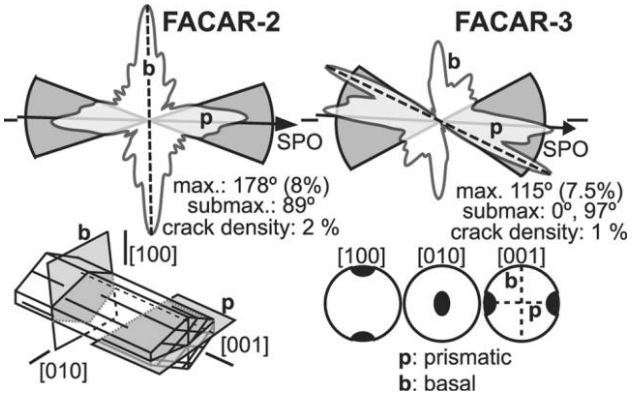

Figure 12. Hornblende microcrack analysis in samples FACAR-2 and 3. Microcrack traces were measured on thin section (*XZ*). The angle to the sample reference axis *X* was used to plot rose diagrams, where cracks were grouped in two orientation sets: basal microcracks (*b*), oriented at a high angle to the [*001*] axis, and prismatic microcracks (*p*), oriented at a low angle to the [*001*] axis. Basal microcracks dominate in sample FACAR-2, while prismatic cracks are more common in FACAR-3. Crack density (crack/grain surface) is higher in sample FACAR-2 (2%).

aries, and only in a few cases do they cross Hbl-Hbl contacts (fig. 6).

Microshear planes quasi-parallel to the main foliation within some plagioclase bands occur in FACAR-3 (*F* in fig. 6*b*4). Grain size reduction and retrogression occur around these planes. A detailed inspection of the grain boundaries reveals grain-boundary sliding microstructures, open voids, and microcracks, all of them indicate grain-boundary sliding. These structures are not penetrative, and sectors affected by them were rejected for EBSD measurements.

Texture. *Amphibole.* Both types of amphibolites developed similar textures (figs. 13, 14). Hornblende has a strong crystallographic-preferred orientation or texture, with an orthorhombic symmetry. The [001] direction is parallel to the lineation (*X*), and (100) planes are parallel to the foliation, while [010] direction defines a maximum centered around the *Y*-axis and elongated in *Z*, which correlates well with previous studies of amphibole textures (e.g., Gapais and Brun 1981; Siegesmund et al. 1989, 1994; Kruhl and Huntemann 1991; Ji and Salisbury 1993; Ji et al. 1993; Barroul and Kern 1996; Ivankina et al. 2005; Díaz Azpiroz et al. 2007; Tatham et al. 2008). Textural analyses from EBSD result in sharper distributions but patterns are equivalent to those obtained using neutron diffraction (figs. 13, 14).

Plagioclase. A comparison of plagioclase textures obtained with EBSD and TOF neutron diffraction from sample FACAR-2 shows important differences (figs. 13*b*, 14). Pole figures derived from EBSD show a spotty and almost random distribution. Neutron diffraction results, however exhibit moderate and consistent textural patterns (maximum/minimum: 2.48/0.18 multiples of a random distribution [m.r.d.]; fig. 14), coherent with the geometry of the flow. Pole figures are complex but some important features arise: all patterns appear rotated against shearing with a monoclinic symmetry, the [010] direction is close to the foliation pole, and the [001] and [100] directions tend to align with the lineation. The plagioclase EBSD texture patterns from FACAR-3 show a dominant [100] direction around the structural lineation, [001] concentrated close to the foliation pole (*Z*), and [010] defining a girdle at 25° to the foliation (fig. 13*a*).

Garnet, Epidote, and Titanite. The garnet from sample FACAR 3 shows no preferred orientation (fig. 13*a*), but EBSD pole figures show elliptical maxima defining crystallographic axes [100], [110], and [111], which suggest plastic distortion of the crystal lattice.

Epidote pole figures (fig. 14) from neutron diffraction (FACAR-2) show a slightly monoclinic fabric (max/min: 3.71/0.23 m.r.d.), consistent with the sense of shearing. The [010] axes define a complex girdle in the *YZ* plane and maxima close to *Z*. The [001] axes concentrate at 45° to the lineation (*X*). Both patterns are coherent with shearing.

The fabric in titanite is strong (maximum/minimum: 6.93/0.02 m.r.d.; fig. 14). Due to its low-volume fraction (~3%), the fabrics in this phase should be interpreted with caution. The [010] direction is distributed in a small circle around lineation (*X*), with a submaximum between *Z* and *X* and [100] and [001] defining complex girdles at a high angle to the foliation. Monoclinic symmetry is consistent with the sense of shear.

Discussion

Origin and Meaning of Textures and Microstructures. The interpretation of textures and microstructures in polyphase deformed rocks is complicated, especially if low-symmetry phases and complex chemical compositions are involved. In amphibolites, both these factors must be considered, so that quantitative textural analysis as well as phase distribution and chemically enhanced features should be evaluated (Brodie and Rutter 1985; Kenkmann and Dresen 2002).

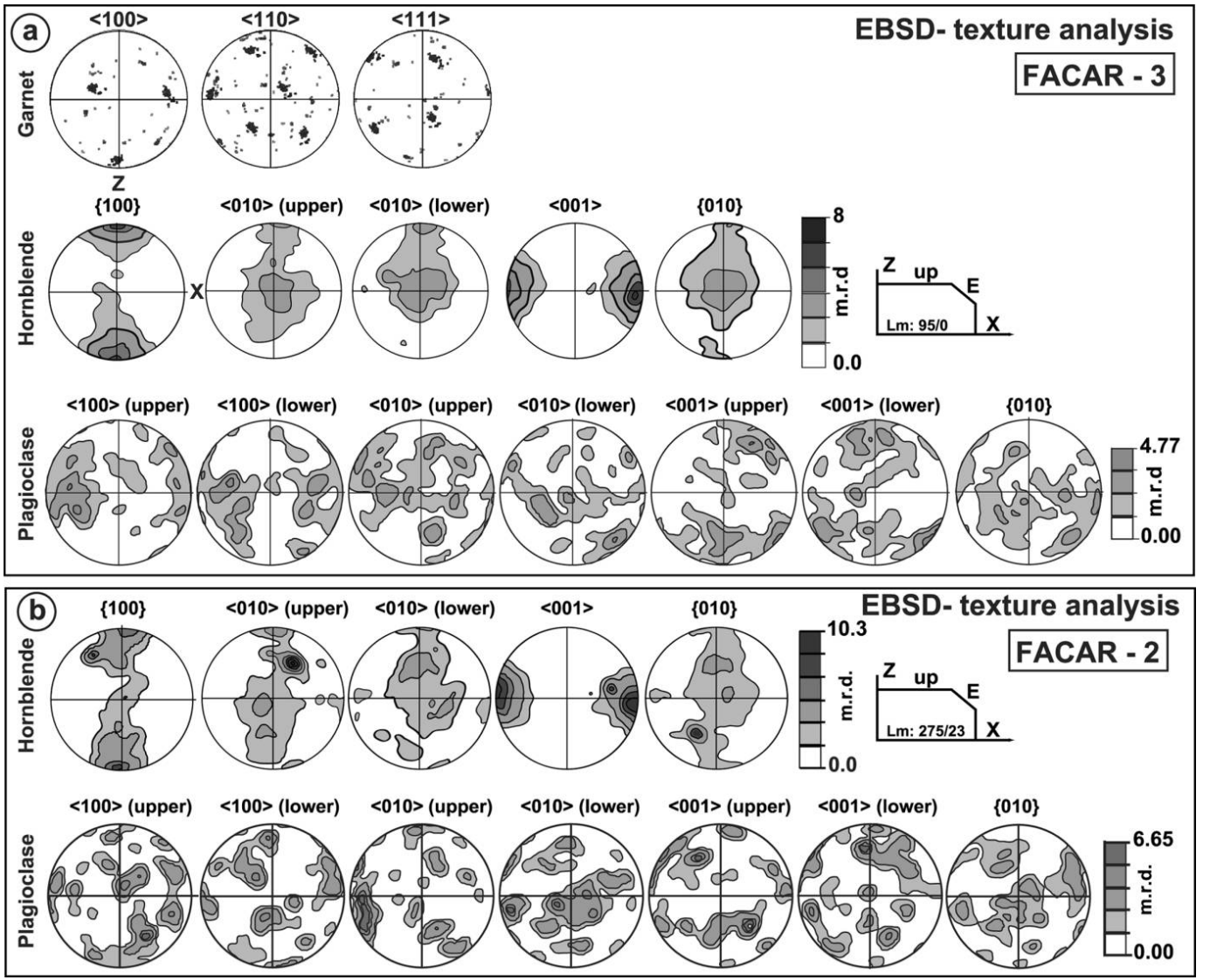

Figure 13. Pole figures from electron backscattered diffraction (EBSD) texture analyses of a high-temperature shear zone (FACAR-3; *a*) and a shear zone inside the thrust sheet at the crustal/mantle boundary (FACAR-2; *b*). Equal area projection. Linear contours: units in multiples of a random distribution (*m.r.d.*). Reference system as in figures 4 and 7.

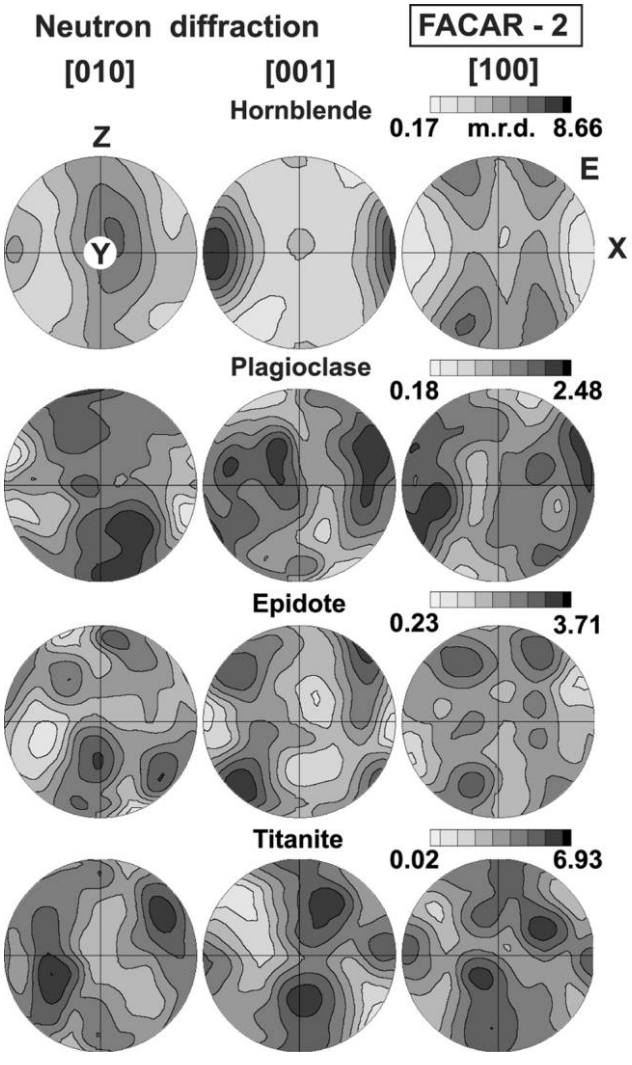

Figure 14. Pole figures from time-of flight (TOF) neutron diffraction analyses of sample FACAR-2. Equal area projection. Log contours: units in multiples of a random distribution (*m.r.d.*). Reference system as in figures 4 and 7.

Hornblende. There is still no agreement about the prevalence of mechanisms during the natural deformation of clinoamphiboles. Available natural and experimental data suggest that different mechanisms cooperate to accomplish this deformation. Crystal-plastic mechanisms (e.g. dislocation glide, dynamic recrystallization, dislocation creep, and subgrain formation) may be dominant under medium- to high-temperature conditions, with (*hk*0) [001] as a major slip system (Rooney et al. 1975; Biermann and Van Roermund 1983; Cumbest et al. 1989; Reynard et al. 1989; Hacker and Christie 1990; Skrotzki 1990, 1992; Kenkmann and Dresen 2002; Baratoux et al. 2005). As the temperature decreases, other mechanisms such as twining, solution mass transfer, and dissolution–precipitation creep become more important (e.g., Dollinger and Blacic 1975; Biermann 1981; Imon et al. 2002). A dominant brittle behavior, with minor solution mass transfer, is documented under lower-temperature conditions (Allison and La Tour 1977; Brodie and Rutter 1985; Nyman et al. 1992; Lafrance and Vernon 1993; Stünitz 1993; Babaie and La Tour 1994; Berger and Stünitz 1996; Imon et al. 2004; Díaz Azpiroz et al. 2007). Rigid-body rotation (Ildefonse et al. 1990; Shelley 1994; Berger and Stünitz 1996; Díaz Azpiroz et al. 2007; Tatham et al. 2008) and solution transfer-oriented growth (Shelley 1989) have been recognized as an effective mechanisms for textural and SPO development at low metamorphic grade.

In sample FACAR-3, textural patterns and the indications of intracrystalline plasticity suggest that the preferred orientation was mainly due to dislocation glide in the [001] (*hk*0) system, probably [001](100) (fig. 13). The presence of small grains of plagioclase and hornblende along large hornblende crystals with concave boundaries points to the activation of grain-boundary migration and heterogeneous nucleation (Kenkmann 2000; Kenkmann and Dresen 2002). However, other mechanisms may have been also important. The SR/α correlation suggests that rigid body rotation occurred (Ildefonse et al. 1990; Shelley 1994). Documented crystal microcracks might be linked to rigid rotation, facilitating grain interactions (Ildefonse et al. 1992; Díaz Azpiroz et al. 2007). These mechanisms could help fabric development, thereby enhancing the strong correlation of SPO and texture (Shelley 1994; Baratoux et al. 2005; Díaz Azpiroz et al. 2007).

Amphiboles in sample FACAR-2 rarely show evidence of crystal plasticity. The strong crystallographic-preferred orientation (in terms of m.r.d.; figs. 13, 14) could be dominantly the result of rigid-body rotation, with minor contribution of dislocation glide parallel to the [001](100) system (figs. 13, 14). The grain boundaries are straight and clear, favoring this interpretation (fig. 6). The presence of abundant microcracks, more than in FACAR-3, also support the idea, where cyclic rigid rotation and microcracking may lead to grain-size reduction and fabric reinforcement (fig. 12). Oriented growth (Shelley 1989) was active during retrogression, as can be seen from the syntaxial development of crescent zones (fig. 9); their presence seems related to amphibole/plagioclase layer boundaries, probably enhanced by chemical gradients around those sectors (Berger and Stünitz 1996) during the retrogression stage. Oriented growth probably helped to am-

plify the rock fabric (i.e., SR, SPO, texture) and the fabric orthorhombic symmetry (Bons and den Brok 2000).

Plagioclase. High-temperature experiments, studies of preferred orientations in naturally deformed high-grade rocks, and simulations all suggest that plagioclase dominantly deforms by dislocation glide on (010)[001] accompanied by (010)[100] slip (Lafrance et al. 1998; Ji et al. 2000, 2004; Stünitz et al. 2003; Gómez Barreiro et al. 2007*a*; Harigane et al. 2008). Slip on (001)[100] has been also identified in naturally deformed rocks at medium- to high-grade conditions (Kruhl 1987; Siegesmund et al. 1994; Terry and Heidelbach 2006; Harigane et al. 2008). Both slip systems have been observed under TEM (Marshall and McLaren 1977; Olsen and Kohlstedt 1984; Montardi and Mainprice 1987).

Plagioclase shows evidence of plastic deformation and dynamic recrystallization in both samples. In FACAR-3 (fig. 6*b*), although the EBSD textural patterns are somewhat complex (fig. 13*a*), some general trends are evident. The [100] axes align with the flow direction (*X*), and the (001) poles are close to the foliation pole (*Z*), being slightly asymmetric. Meanwhile, (010) poles define a girdle at an acute angle to the foliation, opposite to the sense of shearing (fig. 13*a*). These features and geological conditions are compatible with the slip of dislocations on the [100](001) system. On the other hand, the competition of grain growth and the grain-size reduction mechanism during dynamic recrystallization might be considered responsible for the weak SPO (SR~1), and the lognormal grain-size distribution (Michibayashi 1993; Michibayashi and Masuda 1993; Shigematsu 1999; Shimizo 2003; Kellermann Slotemaker 2006). Active grain-boundary migration explains the interlobate shapes (fig. 6*b*) and indicates heterogeneous strain within the aggregate (Ji et al. 2005). It is probable that other mechanisms such as diffusive mass transport assisted deformation and recrystallization (Gómez Barreiro et al. 2007*a*). No evidence of dissolution-precipitation creep, such as chemical zoning, has been found.

The plagioclase in FACAR-2 shows the smallest grain size of both samples. There is evidence of plastic deformation, indicated by the presence of subgrains, twins, and undulose extinction (fig. 6*a*). Recrystallization mechanisms include grain-boundary mobility and may be related to diffusional processes and solution transfer, which led to the sinkynematic development of overgrowths, particularly in those faces perpendicular to the flow direction (*X*). The development of overgrowths might be the reason why plagioclase SPO appears slightly more defined than in sample FACAR-3 (SR/α; fig. 8). Other reactions, triggered by this mechanism, include the growth of epidote, and the actinolitic overgrowths on hornblende. The very low SR of crystals and the pole figure patterns indicate that texture can be attributed to dislocation slip on (010)[001]/[100] system. The (010)[001] system has been documented as the principal slip system under amphibolite and granulite facies conditions (Olsen and Kohlstedt 1984, 1985; Ji and Mainprice 1988; Ji et al. 1988; Ague et al. 1990; Kruse and Stünitz 1999; Kruse et al. 2001). Slip on (010)[100] has been proposed in high-temperature deformation experiments and natural mylonites (Ji et al. 2000, 2004; Gómez Barreiro et al. 2007*a*; Harigane et al. 2008). Experiments by Ji et al. (2005) suggest a transition from [001] to [100] with increasing temperature, strain rate, and water content.

Age Constraints and Geodynamic Implications. Our results can be interpreted in terms of two stages (fig. 5). (1) An early deformation stage, under high-temperature amphibolites facies conditions (>600°C), resulted in plastic deformation of hornblende and plagioclase. Most of the microstructural evolution of the high-temperature shear zones (FACAR-3) occurred at this stage. (2) A late, lower-temperature, late kinematic cooling stage resulted in complex competition of mechanisms, where dislocation glide in amphibole became a secondary mechanism, whereas rigid-body rotation, microcracking, and solution transfer, driven by chemical gradients, became primarily responsible for the shape and crystallographic fabrics. Textural analysis in plagioclase supports the activity of dislocations by slip on the (010)[001] system, which suggests deformation conditions over 550°C (Ji et al. 2005). At lower temperatures, other mechanisms, like dissolution-precipitation creep, contributed to the development of the SPO, without a clear effect on texture. Fabric symmetry points to a top-to-the-east sense of shear during this stage. Most of the microstructural evolution of the inner shear zones (FACAR-2) may have developed during this stage.

Available age determinations in the Careón ophiolite and equivalent units in northwest Iberia, include dating of the amphibolite-facies regional foliation. Widely accepted results include $^{40}Ar/^{39}Ar$ ages that range between 390 and 376 Ma (hornblende concentrates; Dallmeyer and Gil Ibarguchi 1990; Peucat et al. 1990; Dallmeyer et al. 1991, 1997). These ages are interpreted to date the last cooling through those temperatures required for intracrystalline retention of argon within hornblende

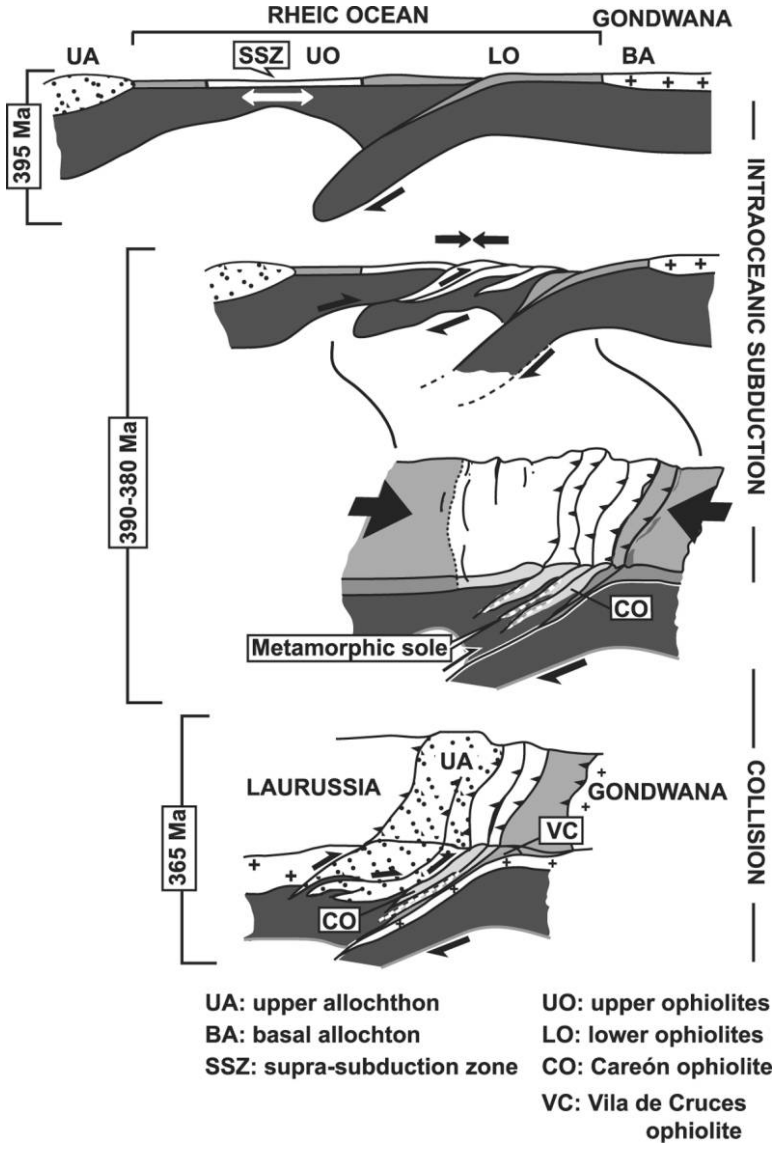

Figure 15. Geodynamic evolution of the Careón ophiolite and related units. Protolith ages from the suprasubduction zone Careón ophiolite (395 Ma) represent an upper age limit for fabric development in the metabasites. The imbrication within an oceanic environment (390–380 Ma) led to the formation of metamorphic soles that currently separate tectonic slices in the unit. The subsequent collisional assemblage (365 Ma) included upper and basal allochthonous units and ophiolitic units along the Variscan suture in northwest Iberia. Based on Arenas et al. (2007*b*), Sánchez Martínez et al. (2007), Gómez Barreiro et al. (2007*a*), and this study.

grains (525° ± 25°C; Harrison 1981). Quoted geochronological experiments apparently reveal no significant disturbance of the argon within the hornblende reservoir. Therefore, it is inferred that the conditions for textural development for plagioclase (550°C) and hornblende (>600°C) occurred before 376 Ma. According to the known history of terrane accretion and continental collision in northwest Iberia (Gómez Barreiro et al. 2006, 2007*b*; Sánchez Martínez et al. 2007; Martínez Catalán et al. 2007, 2009), these fabrics would have developed in a precollisional setting within the Rheic Ocean (figs. 2, 15). This idea is also consistent with the origin of metamorphic soles, which are thought to represent relics of high-temperature intraoceanic thrusts, related to the initial stages of the intraoceanic subduction system (Jamieson 1986; Hacker 1994; Marquer et al. 1995, 1998; Polat et al. 1996).

A correlation can be tentatively established with current subduction systems on the basis of statis-

tical analysis and experimental works (e.g., Uyeda and Kanamori 1979; Jarrard 1986; Boutelier et al. 2003; Heuret et al. 2007). The intraoceanic subduction system developed within the Rheic Ocean included (fig. 15) at least (1) a period of extension in the upper plate, which led to the formation of new oceanic lithosphere (ca. 395 Ma; fig. 15). Shortly afterward (2) the strain state of the upper plate changed to compression, and ductile thrusts developed within the suprasubduction zone lithosphere (ca. 390–380 Ma; fig. 15). Finally (3), the collisional stage started with the subduction of the outermost border of Gondwana at ca. 365 Ma. Subduction systems where upper plate compression occurs are not common in current subduction zones and may involve continental (Chile) and oceanic (Japan) overriding plates (e.g., Heuret and Lallemand 2005; Heuret et al. 2007). It has been recognized that upper plate deformation depends on several internal parameters such as relative motion and velocities of the upper plate, trench, and subducting slab (Conrad et al. 2004; Lallemand et al. 2005; Heuret et al. 2007). Spatial and temporal variations of those parameters may lead to drastic changes not only on the upper plate stress state but also on the subduction geometry (e.g., northwest Pacific subduction zone; Heuret and Lallemand 2005; Heuret et al. 2007). These observations are coherent with precollisional evolution of the Careón ophiolite.

On the basis of fabric evolution within the Careón ophiolite, we suggest (fig. 16) that the imbrication of oceanic lithosphere in the intraoceanic subduction zone imposed a deformation on each tectonic slice, which progressed from outer high-strain boundaries, (early high-*T* shear zones of FACAR-3 type) to inner shear zones (FACAR-2 type) with decreasing temperature. It is important to note that deformation process recorded by the two samples seem to be continuous, with a common west-east vector (present coordinates) and similar kinematics. This contrasts with the northwest-southeast kinematics of the thrusts that emplaced the ophiolitic units above the northwest Iberian allochthon during the Variscan collision (Martínez Catalán et al. 2002). Structural overprinting due to exhumation by thrusting and postemplacement events is limited to discrete and low-grade structures that did not disturb the plastic fabric.

Conclusions

Quantitative textural analysis through EBSD, TOF neutron diffraction, and microstructural characterization were conducted in two distinct mylonitic metabasites from the crustal section of the Careón ophiolite (northwest Spain) in order to constrain the origin, evolution, and geodynamic significance of deformation fabrics. Early high-temperature (>600°C) shear zones developed in metamorphic soles at thrust boundaries display textures and microstructures that were probably generated through dislocation glide, by slip on [001] (100) and [100] (001) in hornblende and plagioclase, respectively. Dynamic recrystallization was also active during deformation. Inferences based on thermobarometry and thermal constraints on suggested slip systems are in good agreement. Lower temperature overprints (rigid-rotation hornblende) resulted in a reinforcement of the fabric.

Shear zones developed at lesser temperature in the inner parts of the thrust sheets, and display fabrics that predominantly developed by rigid-body rotation of hornblende with a minor contribution of dislocation glide on [001](100). Crystallographic-preferred orientation of plagioclase was accomplished by dislocation glide on [001](010). These findings are coherent with temperature estimates between over 550°C and 600°C. Solution transfer mechanisms and synkinematic reactions led to an enhancement of shape fabric at even lower temperatures.

Thermal constraints based on texture and microstructural features point to a development of the mylonitic fabric under higher temperatures than the argon retentive thermal limit for hornblende. This interpretation supports an early Variscan, precollisional age for the higher-temperature fabrics, probably in the intraoceanic subduction setting suggested for the Rheic Ocean during the Devonian.

Our results indicate that a precollisional, continuous evolution of fabric development has been recorded in the Careón ophiolite. These fabrics represent the early stages of the closure of the Rheic Ocean with a constant west-east flow direction (in present coordinates). The orientation of the regional lineation and related kinematic criteria may be tentatively used to infer relative motions of the plates involved in the Variscan suture of northwest Iberia, and it may be considered a reference vector for convergence models in this part of the Variscan orogen. The combination of quantitative texture and microstructural analysis is confirmed as an important tool in order to extract information from polymineralic rocks and connect the different observation scales and data sources in tectonic studies.

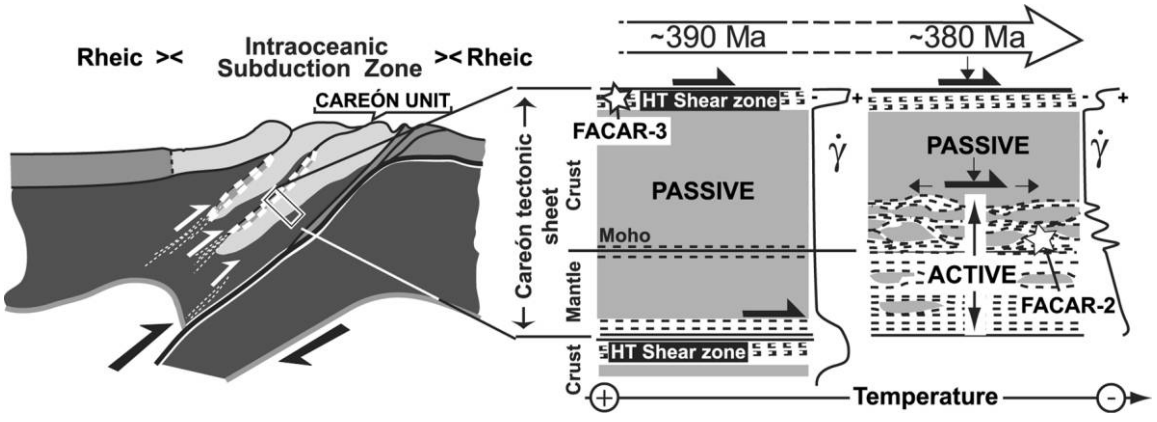

Figure 16. Conceptual model (not to scale) for the evolution of tectonic fabrics within the Careón Unit. In an early stage of intraoceanic subduction and imbrication (390 Ma), deformation mostly concentrated on slice boundaries, where metamorphic soles developed (*white dashed lines*, in the geological section), and in high-temperature shear zones in the crustal section (sample FACAR-3), while most of the oceanic crust remained unaffected. In a later stage (380 Ma), deformation penetrated inside the unit and lithological boundaries such as the crust/mantle transition (Moho) concentrated an important part of the deformation (sample FACAR-2).

ACKNOWLEDGMENTS

We acknowledge support from the National Science Foundation, the U.S. Department of Energy, and research projects CGL2007-65338-CO2-01 and 02/BTE of the Dirección General de Programas y Transferencia del Conocimiento (Spanish Ministry of Science and Innovation). Access to the Los Alamos Neutron Science Center (LANSCE) High-Pressure Preferred-Orientation Diffractometer (HIPPO) to perform texture measurements was invaluable. J. Gómez Barreiro was supported by post-doctoral contracts (Spanish Ministerio de Educación y Ciencia [MEC] EX-2005-0490 and MEC–Juan de la Cierva). We are grateful to B. Murphy and S. T. Johnston for thorough and constructive reviews and to D. B. Rowley for the editorial work.

REFERENCES CITED

Abbatte, E.; Bortolotti, V.; Passerini, P. ; and Principi, G. 1985. The rhythm of Phanerozoic ophiolites. Ofioliti 10:109–138.

Agard, P.; Jolivet, L.; Vrielynck, B.; Burov, E.; and Monié, P. 2007. Plate acceleration: the obduction trigger? Earth Planet. Sci. Lett. 258:428–441.

Ague, M. D.; Wenk, H. R.; and Wenk, E. 1990. Deformation microstructures and lattice orientations of plagioclase in gabbros from central Australia. Geophys. Monogr. 56:173–186.

Aitchison, J. C.; Badengzhu; Davis, A. M.; Liu, J.; Luo, H.; Malpas, J. G.; McDermid, I. R. C.; Wu, H.; Ziabrev, S. V.; and Zhou, M. 2000. Remnants of a Cretaceous intra-oceanic subduction system within the Yarlung-Zangbo suture (southern Tibet). Earth Planet. Sci. Lett. 183:231–244.

Allison, I., and La Tour, T. E. 1977. Brittle deformation of hornblende in a mylonite: a direct geometrical analogue of ductile deformation by translation gliding. Can. J. Earth Sci. 14:1953–1958.

Anderson, J. L., and D. R. Smith. 1995. The effects of temperature and fO_2 on the Al-in-hornblende barometer. Am. Mineral. 80:549–559.

Arenas, R.; Martínez Catalán, J. R.; Sánchez Martínez, S.; Díaz García, F.; Abati, J.; Fernández-Suárez, J.; Andonaegui, P.; and Gómez-Barreiro, J. 2007*a*. Paleozoic ophiolites in the Variscan suture of Galicia (northwest Spain): distribution, characteristics, and meaning. *In* Hatcher, R. D., Jr., ; Carlson, M. P.; McBride, J. H.; and Martínez Catalán, J. R., eds. 4-D framework of continental crust. Geol. Soc. Am. Mem. 200:425–444.

Arenas, R.; Martínez Catalán, J. R.; Sánchez Martínez, S.; Fernández-Suárez, J.; Andonaegui, P.; Pearce, J. A.; and Corfu, F. 2007*b*. The Vila de Cruces ophiolite: a remnant of the early Rheic Ocean in the Variscan suture of Galicia (northwest Iberian Massif). J. Geol. 115: 129–148.

Babaie, H. A., and La Tour, T. E. 1994. Semibrittle and cataclastic deformation of hornblende-quartz rocks in a ductile shear zone. Tectonophysics 229:19–30.

Baratoux, L.; Schulmann, K.; Ulrich, S.; and Lexa, O. 2005. Contrasting microstructures and deformation

mechanisms in metagabbro mylonites contemporaneously deformed under different temperatures (c. 650°C and c. 750°C). *In* Gapais, D.; Brun, J. P.; and Cobbold, P. R., eds. Deformation mechanisms, rheology and tectonics: from minerals to the lithosphere. Geol. Soc. Spec. Publ. 243:97–125.

Barroul, G., and Kern, H. 1996. Seismic anisotropy and shear-wave splitting in lower-crustal and upper-mantle rocks from the Ivrea Zone: experimental and calculated data. Phys. Earth Planet. Inter. 95:175–194.

Beccaluva, L.; Coltorti, M.; Guiunta, G.; and Siena, F. 2004. Tethyan vs. cordilleran ophiolites: a reappraisal of distinctive tectono-magmatic features of supra-subduction complexes in relation to the subduction mode. Tectonophysics 393:163–174.

Berger, A., and Stünitz, H. 1996. Deformation mechanisms and reaction of hornblende: examples from the Bergell tonalite (Central Alps). Tectonophysics 257: 149–174.

Berly, T. J.; Hermann, J.; Arculus, R. J.; and Lapierre, H. 2006. Supra-subduction zone pyroxenites from San Jorge and Santa Isabel (Solomon Islands). J. Petrol. 47: 1531–1555.

Biermann, C. 1981. (100) deformation twins in naturally deformed amphiboles. Nature 292:821–823.

Biermann, C., and H. L. M. Van Roermund. 1983. Defect structures in naturally deformed clinoamphiboles: a TEM study. Tectonophysics 95:267–278.

Bons, P. D., and den Brok, B. W. J. 2000. Crystallographic preferred orientation development by dissolution precipitation creep. J. Struct. Geol. 22:1713–1722.

Boudier, F.; Bouchez, J. L.; Nicolas, A.; Cannat, M.; Ceuleneer, G.; Miseri, M.; and Montigny, R. 1985. Kinematics of oceanic thrusting in the Oman ophiolites: model of plate convergence. Earth Planet. Sci. Lett. 75:215–222.

Boudier, F.; Ceuleneer, G.; and Nicolas, A. 1988. Shear zones, thrusts and related magmatism in the Oman ophiolite: initiation of thrusting on an oceanic ridge. Tectonophysics 151:275–296.

Boutelier, D.; Chemenda, A.; and Burg, J.-P. 2003. Subduction versus accretion of intra-oceanic volcanic arcs: insight from thermo-mechanical analogue experiments. Earth Planet. Sci. Lett. 212:31–45.

Brodie, K. H., and Rutter, E. H. 1985. On the relationship between deformation and metamorphism, with special reference to the behaviour of basic rocks. *In* Thompson, A. B., and Rubie, D. C., eds. Metamorphic reactions: kinetics, textures and deformation. New York, Springer, p. 138–179.

Castro, A.; Fernández, C.; de la Rosa, J. D.; Moreno-Ventas, I.; and Rogers, G. 1996. Significance of MORB-derived amphibolites from the Aracena metamorphic belt, southwest Spain. J. Petrol. 37:235–260.

Ceuleneer, G.; Nicolas, A.; and Boudier, F. 1988. Mantle flow patterns at an oceanic spreading centre: the Oman peridotites record. Tectonophysics 151:1–26.

Cocks, L. R. M., and Torsvik, T. H. 2002. Earth geography from 500 to 400 million years ago: a faunal and paleomagnetic review. J. Geol. Soc. (Lond.) 159:631–644.

Conrad, C. P.; Bilek, S.; and Lithgow-Bertelloni, C. 2004. Great earthquakes and slab pull: interaction between seismic coupling and plate-slab coupling. Earth Planet. Sci. Lett. 218:109–122.

Cumbest, R. J.; van Roermund, H. L. M.; Drury, M. R.; and Simpson, C. 1989. Burgers vector determination in clinoamphibole by computer simulation. Am. Mineral. 74:586–592.

Dallmeyer, R. D., and Gil Ibarguchi, J. I. 1990. Age of amphibolitic metamorphism in the ophiolitic unit of the Morais allochthon (Portugal): implications for early Hercynian orogenesis in the Iberian Massif. J. Geol. Soc. (Lond.) 147:873–878.

Dallmeyer, R. D.; Martínez Catalán, J. R.; Arenas, R.; Gil-Ibarguchi, J. I.; Gutiérrez Alonso, G.; Farias, P.; Aller, J.; and Bastida, F. 1997. Diachronous Variscan tectonothermal activity in the NW Iberian Massif: evidence from $^{40}Ar/^{39}Ar$ dating of regional fabrics. Tectonophysics 277:307–337.

Dallmeyer, R. D.; Ribeiro, A.; and Marques, F. 1991. Polyphase Variscan emplacement of exotic terranes (Morais and Bragança) onto Iberian succesions: evidence from $^{40}Ar/^{39}Ar$ mineral ages. Lithos 27:133–144.

Davies, G. F., and Richards, M. A. 1992. Mantle convection. J. Geol. 100:151–206.

Díaz Azpiroz, M.; Lloyd, G. E.; and Fernández, C. 2007. Development of lattice preferred orientation in clinoamphiboles deformed under low-pressure metamorphic conditions—a SEM/EBSD study of metabasites from the Aracena metamorphic belt, SW Spain. J. Struct. Geol. 29:629–645.

Díaz García, F.; Arenas, R.; Martínez Catalán, J. R.; González del Tánago, J.; and Dunning, G. 1999. Tectonic evolution of the Careón ophiolite (northwest Spain): a remnant of oceanic lithosphere in the Variscan belt. J. Geol. 107:587–605.

Dilek, Y., and Newcomb, S., eds. 2003. Ophiolite concept and the evolution of geological thought. Geol. Soc. Am. Mem. 373, 504 p.

Doglione, C.; Carminati, E.; Cuffaro, M.; and Scrocca, D. 2007. Subduction kinematics and dynamic constraints. Earth Sci. Rev. 83:125–175.

Dollinger, G., and Blacic, J. D. 1975. Deformation mechanisms in experimentally and naturally deformed amphiboles. Earth Planet. Sci. Lett. 26:409–416.

Dubińska, E.; Bylina, P.; Kozlowski, A.; Dörr, W.; and Nejbert, K. 2004. U-Pb dating of serpentinization: hydrothermal zircon from a metasomatic rodingite shell (Sudetic ophiolite, SW Poland). Chem. Geol. 203:183–203.

Fitz Gerald, J. D.; Parise, J. B.; and Mackinnon, I. D. R. 1986. Average structure of an An^{48} plagioclase from the Hogarth Ranges. Am. Mineral. 71:1399–1408.

Gabe, E. J.; Porheine, J. C.; and Whitlow, S. H. 1973. A reinvestigation of the epidote structure: confirmation of the iron location. Am. Mineral. 58:218–223.

Gapais, D., and Brun, J.-P. 1981. A comparison of mineral grain fabrics and finite strain in amphibolites from eastern Finland. Can. J. Earth Sci. 18:995–1003.

Godard, M.; Jousselin, D.; and Bodinier, J.-L. 2000. Re-

lationships between geochemistry and structure beneath a palaeo-spreading centre: a study of the mantle section in the Oman ophiolite. Earth Planet. Sci. Lett. 180:133–148.

Gómez Barreiro, J.; Lonardelli, I.; Wenk, H.-R.; Dresen, G.; Rybacki, E.; Ren, Y.; and Tomé, C. N. 2007*a*. Preferred orientation of anorthite deformed experimentally in Newtonian creep. Earth Planet. Sci. Lett. 264: 188–207.

Gómez Barreiro, J.; Martínez Catalán, J. R.; Arenas, R.; Castiñeiras, P.; Abati, J.; Díaz García, F.; and Wijbrans, J. R. 2007*b*. Tectonic evolution of the upper allochthon of the Órdenes complex (northwestern Iberian Massif): structural constraints to a polyorogenic peri-Gondwanan terrane. *In* Linnemann, U.; Nance, R. D.; Kraft, P.; and Zulauf, G., eds. The evolution of the Rheic Ocean: from Avalonian-Cadomian active margin to Alleghenian-Variscan collision. Geol. Soc. Am. Spec. Pap. 423:315–332.

Gómez Barreiro, J.; Wijbrans, J. R.; Castiñeiras, P.; Martínez Catalán, J. R.; Arenas, R.; Díaz García, F.; and Abati, J. 2006. $^{40}Ar/^{39}Ar$ laserprobe dating of mylonitic fabrics in a polyorogenic terrane of the NW Iberia. J. Geol. Soc. (Lond.) 163:61–73

Hacker, B. R. 1994. Rapid emplacement of young oceanic lithosphere: argon geochronology of the Oman ophiolite. Science 265:1563–1565.

Hacker, B. R., and Christie, J. M. 1990. Brittle/ductile and plastic/cataclastic transition in experimentally deformed and metamorphosed amphibolite. *In* Duba, A. G.; Durham, W. B.; Handin, J. W.; and Wang, H. F., eds. The brittle-ductile transition in rocks. Am. Geophys. Union Geophys. Monogr., p. 127–148.

Hacker, B. R., and Mosenfelder, J. L. 1996. Metamorphism and deformation along the emplacement thrust of the Samail ophiolite, Oman. Earth Planet. Sci. Lett. 144:435–451.

Handy, M. R. 1994. Flow laws for rocks containing 2 nonlinear viscous phases: a phenomenological approach. J. Struct. Geol. 16:287–301.

Harigane, Y.; Michibayashi, K.; and Ohara, Y. 2008. Shearing within lower crust during progressive retrogression: structural analysis of gabbroic rocks from the Godzilla Mullion, an oceanic core complex in the Parece Vela backarc basin. Tectonophysics 457:183–196.

Harrison, T. M. 1981. Diffusion of ^{40}Ar in hornblende. Contrib. Mineral. Petrol. 78:324–331.

Heilbronner, R., and D. Bruhn 1998. The influence of three-dimensional grain size distributions on the rheology of polyphase rocks. J. Struct. Geol. 20:695–705.

Heuret, A.; Funiciello, F.; Faccenna, C.; and Lallemand, S. 2007. Plate kinematics, slab shape and back-arc stress: a comparison between laboratory models and current subduction zones. Earth Planet. Sci. Lett. 256: 473–483.

Heuret, A., and Lallemand, S. 2005. Plate motions, slab dynamics and back-arc deformation. Phys. Earth Planet. Inter. 149:31–51.

Holdaway, M. J. 1971. Stability of andalusite and the aluminum silicate phase diagram. Am. J. Sci. 271:97–131.

Holland, T. J. B., and Blundy, J. D. 1994. Non-ideal interactions in calcic amphiboles and their bearing on amphibole-plagioclase thermometry. Contrib. Mineral. Petrol. 116:433–447.

Ildefonse, B.; Lardeaux, J. M.; and Caron, J. M. 1990. The behavior of shape preferred orientations in metamorphic rocks: amphiboles and jadeites from the Monte Mucrone area (Sesia-Lanzo zone, Italian Western Alps). J. Struct. Geol. 12:1005–1011.

Ildefonse, B.; Launeau, P.; Bouchez, J. L.; and Fernandez, A. 1992. Effect of mechanical interactions on the development of shape preferred orientations: a two-dimensional experimental approach. J. Struct. Geol. 14:73–83.

Imon, R.; Okudaira, T.; and Fujimoto, A. 2002. Dissolution and precipitation processes in the deformed amphibolites: an example from the ductile shear zone of the Ryoke metamorphic belt, SW Japan. J. Metamorph. Geol. 20:297–308.

Imon, R.; Okudaira, T.; and Kanagawa, K. 2004. Development of shape- and lattice-preferred orientations of amphibole grains during cataclastic deformation and subsequent deformation by dissolution-precipitation creep in amphibolites from the Ryoke metamorphic belt, SW Japan. J. Struct. Geol. 26:793–805.

Ivankina, T. I.; Kern, H. M.; and A. N. Nikitin. 2005. Directional dependence of P- and S-wave propagation and polarization in foliated rocks from the Kola superdeep well: evidence from laboratory measurements and calculations based on TOF neutron diffraction. Tectonophysics 407:25–42.

Jähne, B. 1991. Digital image processing, concepts, algorithms and scientific applications. New York, Springer.

Jamieson, R. A. 1986. *P-T* paths from high-temperature shear zones beneath ophiolites. J. Metamorph. Geol. 4:3–22.

Jarrard, R. D. 1986. Relations among subduction parameters. Rev. Geophys. 24:217–284.

Ji, S.; Jiang, Z.; Rybacki, E.; Wirth, R.; Prior, D.; and Xia, B. 2004. Strain softening and microstructural evolution of anorthite aggregates and quartz-anorthite layered composites deformed in torsion. Earth Planet. Sci. Lett. 222:377–390.

Ji, S., and Mainprice, D. 1988. Natural deformation fabrics of plagioclase: implications for slip systems and seismic anisotropy. Tectonophysics 147:145–163.

Ji, S.; Mainprice, D.; and Boudier, F. 1988. Sense of shear in high-temperature movement zones from the fabric asymmetry of plagioclase feldspars. J. Struct. Geol. 10: 73–81.

Ji, S.; Rybacki, E.; Wirth, R.; Jiang, Z.; and Xia, B. 2005. Mechanical and microstructural characterization of calcium aluminosilicate (CAS) and SiO_2/CAS composites deformed at high temperature and high pressure. J. Eur. Ceram. Soc. 25:301–311.

Ji, S., and Salisbury, M. H. 1993. Shear-wave velocities,

anisotropy and splitting in high-grade mylonites. Tectonophysics 221:453–473.
Ji, S.; Salisbury, M. H.; and Hammer, S. 1993. Petrofabric, P-wave anisotropy and seismic reflectivity of high-grade tectonites. Tectonophysics 222:195–226.
Ji, S.; Wirth, R.; Rybacki, E.; and Jiang, Z. 2000. High-temperature plastic deformation of quartz-plagioclase multilayers by layer-normal compression. J. Geophys. Res. 105:16,651–16,664.
Kellermann Slotemaker, A. 2006. Dynamic recrystallization and grain growth in olivine rocks. Geologica Ultraiectina 268. Alblasserdam, Offsetdrukkerij Kanters, 187 p.
Kenkmann, T. 2000. Processes controlling the shrinkage of porphysoclats in gabbroic shear zones. J. Struct. Geol. 22:471–487.
Kenkmann, T., and Dresen, G. 2002. Dislocation microstructure and phase distribution in a lower crustal shear zonean example from the Ivrea Zone, Italy. Int. J. Earth Sci. 91:445–458.
King, S. D. 2001. Subduction zones: observations and geodynamic models. Phys. Earth Planet. Inter. 127:9–24.
Kretz, R. 1983. Symbols for rock-forming minerals. Am. Mineral. 68:277–279.
Kruhl, J. H. 1987. Preferred lattice orientations of plagioclase from amphibolite and greenschist facies rocks near the Insubric Line (Western Alps). Tectonophysics 135:233–242.
Kruhl, J. H., and Huntemann, T. 1991. The structural state of the former lower continental crust in Calabria (S. Italy). Geol. Rundsch. 81:289–302.
Kruse, R., and Stünitz, H. 1999. Deformation mechanisms and phase distribution in mafic high-temperature mylonites from the Jotun Nappe, southern Norway. Tectonophysics 303:223–249.
Kruse, R.; Stünitz, H.; and Kunze, K. 2001. Dynamic recrystallization processes in plagioclase porphyroclasts. J. Struct. Geol. 23:1781–1802.
Lafrance, B.; John, B. E.; and Frost, B. R. 1998. Ultra high-temperature and subsolidus shear zones: examples from the Poe Mountain anorthosite, Wyoming. J. Struct. Geol. 20:945–955.
Lafrance, B., and Vernon, R. H. 1993. Mass transfer and microfracturing in gabbroic mylonites of the Guadalupe igneous complex, California. *In* Boland, J. N., and Fitz Gerald, J. D., eds. Defects and processes in the solid state: geoscience applications: the McLaren volume (Developments in Petrology, Vol. 4). Amsterdam, Elsevier Science, p. 151–167.
Lallemand, S.; Heuret, A.; and Boutelier, D. 2005. On the relationships between slab dip, back-arc stress, upper plate absolute motion, and crustal nature in subduction zones. Geochem. Geophys. Geosyst. 6, Q09006, doi:10.1029/2005GC000917.
Launeau, P., and Cruden, A. R. 1998. Magmatic fabric acquisition mechanisms in a syenite: results of a combined anisotropy of magnetic susceptibility and image analysis study. J. Geophys. Res. 103:5067–5089.
Launeau, P., and Robin, P.-Y. F. 1996. Fabric analysis using the intercept method. Tectonophysics 267:91–119.
Leake, B. E. 1978. Nomenclature of amphiboles. Am. Mineral. 63:1023–1052.
Leake, B. E.; Woolley, A. R.; Birch, W. D.; Burke, E. A. J.; Ferraris, G.; Grice, J. D.; Hawthorne, F. C., et al. 2004. Nomenclature of amphiboles: additions and revisions to the International Mineralogical Association's amphibole nomenclature. Am. Mineral. 89:883–887.
Leiss, B.; Groeger, H. R.; Ullemeyer, K.; and Lebit, H. 2002. Textures and microstructures of naturally deformed amphibolites from the northern Cascades, NW USA. *In* De Meer, S.; Drury, M. R.; De Bresser, J. H. P.; and Pennock, G. M., eds. Deformation mechanisms, rheology and tectonics: current status and future perspectives. Geol. Soc. Am. Spec. Publ. 200:219–238.
Lutterotti, L.; Matthies, S.; and Wenk, H.-R. 1999. MAUD: a friendly Java program for materials analysis using diffraction. Int. Union Crystallogr. Comm. Powder Diffr. Newsl. 21:14–15.
Marquer, D.; Mercolli, I.; and Peters, T. 1998. Early Cretaceous intra-oceanic rifting in the Proto-Indian Ocean recorded in the Masirah Ophiolite, Sultanate of Oman. Tectonophysics 292:1–16.
Marquer, D.; Peters, T.; and Gnos, E. 1995. A new structural interpretation for the emplacement of the Masirah ophiolites (Oman): a main Paleocene intra-oceanic thrust. Geodin. Acta 8:13–19.
Marshall, D. B., and McLaren, A. C. 1977. The direct observation and analysis of dislocations in experimentally deformed plagioclase feldspars. J. Mater. Sci. 12:893–903.
Martínez Catalán, J. R.; Arenas, R.; Abati, J.; Sánchez Martínez, S.; Díaz García, F.; Fernández Suárez, J.; González Cuadra, P., et al. 2009. A rootless suture and the loss of the roots of a mountain chain: the Variscan belt of NW Iberia. C. R. Geosci. 341:114–126.
Martínez Catalán, J. R.; Arenas, R.; Díaz García, F.; Gómez Barreiro, J.; González Cuadra, P.; Abati, J.; Castiñeiras, P., et al. 2007. Space and time in the tectonic evolution of the northwestern Iberian Massif: implications for the comprehension of the Variscan belt. *In* Hatcher, R. D., Jr.; Carlson, M. P.; McBride, J. H.; and Martínez Catalán, J. R., eds. 4-D framework of continental crust. Geol. Soc. Am. Mem. 200:403–423.
Martínez Catalán, J. R.; Díaz García, F.; Arenas, R.; Abati, J.; Castiñeiras, P.; González Cuadra, P.; Gómez Barreiro, J.; and Rubio Pascual, F. 2002. Thrust and detachment systems in the Ordenes Complex (northwestern Spain): implications for the Variscan-Appalachian geodynamics. *In* Martínez Catalán, J. R.; Hatcher, R. D., Jr.; Arenas, R.; and Díaz García, F., eds. Variscan-Appalachian dynamics: the building of the Late Paleozoic basement. Geol. Soc. Am. Spec. Pap. 364:163–182.
Matthies, S., and Wenk, H.-R. 2009. Transformations for monocellinic crystal symmetry in texture analysis. J. Appl. Cryst. 42:564–571.
McCusker, L. B.; Von Dreele, R. B.; Cox, D. E.; Louer,

D.; and Scardi, P. 1999. Rietveld refinement guidelines. J. Appl. Cryst. 32:36–50.
Michibayashi, K. 1993. Syntectonic development of a strain-independent steady-state grain size during mylonitization. Tectonophysics 222:151–164.
Michibayashi, K., and Mainprice, D. 2004. The role of pre-existing mechanical anisotropy on shear zone development within oceanic mantle lithosphere: an example from the Oman ophiolite. J. Petrol. 45:405–414.
Michibayashi, K., and Masuda, T. 1993. Shearing during progressive retrogression in granitoids: abrupt grain size reduction of quartz at the plastic-brittle transition for feldspar. J. Struct. Geol. 15:1421–1432.
Montardi, Y., and Mainprice, D. 1987. A transmission electron microscopy study of the natural plastic deformation of calcic plagioclase ($An^{68–70}$). Bull. Mineral. 110:1–14.
Murphy, J. B.; Gutiérrez-Alonso, G.; Nance, R. D.; Fernández-Suárez, J.; Keppie, J. D.; Quesada, C.; Strachan, R. A.; and Dostal, J. 2006. Origin of the Rheic Ocean: rifting along a Neoproterozoic suture? Geology 34: 325–328.
Němec, D. 1967. Determination of the character of oriented potash feldspar overgrowth on plagioclase crystals in igneous rocks. Contrib. Mineral. Petrol. 16: 149–155.
Nicolas, A. 1989. Structures in ophiolites and dynamics of oceanic lithosphere, petrology and structural geology. Dordrecht, Kluwer, 367 p.
Nicolas, A.; Boudier, F.; and Ildefonse, B. 1994. Evidence from the Oman ophiolite for active mantle upwelling beneath a fast-spreading ridge. Nature 370:51–53
Nutman, A. P.; Green, D. H.; Cook, C. A.; Styles, M. T.; and Holdsworth, R. E. 2001. SHRIMP U-Pb zircon dating of the exhumation of the Lizard Peridotite and its emplacement over crustal rocks: constraints for tectonic models. J. Geol. Soc. (Lond.) 158:809–820.
Nyman, M. W.; Law, R. D.; and Smelik, E. A. 1992. Cataclastic deformation for the development of core and mantle structures in amphibole. Geology 20:455–458.
Oberti, R.; Ungaretti, L.; Hawthorne, F. C.; and I. Memmi. 1995. Temperature-dependent Al order-disorder in the tetrahedral double chain of C2/m amphiboles. Eur. J. Mineral. 7:1049–1063.
Olsen, T. S., and Kohlstedt, D. L. 1984. Analysis of dislocations in some naturally deformed plagioclase feldspars. Phys. Chem. Mineral. 11:153–160.
———. 1985. Natural deformation and recrystallization of some intermediate plagioclase feldspars. Tectonophysics 111:107–131.
Parkinson, I. J., and Pearce, J. A. 1998. Peridotites from the Izu-Bonin-Mariana Forearc (ODP leg 125): evidence for mantle melting and melt-mantle interaction in a supra-subduction zone setting. J. Petrol. 39:1577–1618.
Pearce, J. A.; Lippard, S. J.; and Roberts, S. 1984. Characteristics and tectonic significance of supra-subduction zone ophiolites. *In* Kokelaar, B. P., and Howells, M. F., eds. Marginal basin geology: volcanic and associated sedimentary and tectonic processes in modern and ancient marginal basins. Geol. Soc. Spec. Publ. 16:77–94.
Pehl, J., and Wenk, H.-R. 2005. Evidence for regional Dauphiné twinning in quartz from the Santa Rosa mylonite zone in southern California: a neutron diffraction study. J. Struct. Geol. 27:1741–1749.
Peucat, J. J.; Bernard-Griffiths, J.; Gil Ibarguchi, J. I.; Dallmeyer, R. D.; Menot, R. P.; Cornichet, J.; and Iglesias Ponce de León, M. 1990. Geochemical and geochronological cross section of the deep Variscan crust: the Cabo Ortegal high-pressure nappe (northwest Spain). Tectonophysics 177:263–292.
Pin, C.; Paquette, J. L.; Santos Zalduegui, J. F.; and Gil Ibarguchi, J. I. 2002. Early Devonian supra-subduction zone ophiolite related to incipient collisional processes in the western Variscan belt: the Sierra de Careón unit, Órdenes complex, Galicia. *In* Martínez Catalán, J. R.; Hatcher, R. D.; Arenas, R.; and Díaz García, F., eds. Variscan-Appalachian dynamics: the building of the Late Paleozoic basement. Geol. Soc. Am. Spec. Pap. 364:57–72.
Polat, A.; Casey, J. F.; and Kerrich, R. 1996. Geochemical characteristics of accreted material beneath the Pozanti-Karsanti ophiolite, Turkey: intra-oceanic detachment, assembly and obduction. Tectonophysics 263:249–276.
Prior, D. J.; Boyle, A. P.; Brenker, F.; Cheadle, M. C.; Day, A.; López, G.; Peruzzo, L., et al. 1999. The application of electron backscatter diffraction and orientation contrast imaging in the SEM to textural problems in rocks. Am. Mineral. 84:1741–1759.
Prior, D. J.; Trimby, P. W.; Weber, U. D.; and Dingley, D. J. 1996. Orientation contrast imaging of microstructures in rocks using forescatter detectors in the scanning electron microscope. Mineral. Mag. 60:859–869.
Prior, D. J., and Wheeler, J. 1999. Feldspar fabrics in a greenschist facies albite-rich mylonite from electron backscatter diffraction. Tectonophysics 303:29–49.
Reynard, B.; Gillet, P.; and Williame, C. 1989. Deformation mechanisms in naturally deformed glaucophanes: a TEM and HREM study. Eur. J. Mineral. 1: 611–624.
Rooney, T. P.; Riecker, R. E.; and Gavasci, A. T. 1975. Hornblende deformation features. Geology 3:364–366.
Sánchez Martínez, S.; Arenas, R.; Díaz García, F.; Martínez Catalán, J. R.; Gómez Barreiro, J.; and Pearce, J. A. 2007. Careón ophiolite, NW Spain: suprasubduction zone setting for the youngest Rheic Ocean floor. Geology 35:53–56.
Searle, M. P., and Cox, J. 1999. Tectonic setting, origin and obduction of the Oman ophiolite. Geol. Soc. Am. Bull. 111:104–122.
Schellart, W. P. 2008. Subduction zone trench migration: slab driven or overriding-plate-driven? Phys. Earth Planet. Inter. 170:73–88.
Schellart, W. P.; Freeman, J.; Stegman, D. R.; Moresi, L.; and May, D. 2007. Evolution and diversity of subduction zones controlled by slab width. Nature 446:308–311.
Schmidt, M. W. 1992. Amphibole composition in tonalite

as a function of pressure: an experimental calibration of the Al-in-hornblende barometer. Contrib. Mineral. Petrol. 110:304–310.

Schmidt, N.-H., and N. O. Olesen 1989. Computer-aided determination of crystal-lattice orientation from electron-channeling patterns in the SEM. Can. Mineral. 27:15–22.

Shelley, D. 1989. Plagioclase and quartz preferred orientation in a low-grade schist: the roles of primary growth and plastic deformation. J. Struct. Geol. 11: 1029–1037.

———. 1994. Spider texture and amphibole preferred orientations. J. Struct. Geol. 16:709–717.

Shigematsu, N. 1999. Dynamic recrystallization in deformed plagioclase during progressive shear deformation. Tectonophysics 305:437–452

Shimizo, I. 2003. Grain size evolution in dynamic recrystallization. Mater. Sci. Forum 426–432:3587–3592.

Siegesmund, S.; Helmig, K.; and Kruse, R. 1994. Complete texture analysis of a deformed amphibolite: comparison between neutron diffraction and U-stage data. J. Struct. Geol. 16:131–142.

Siegesmund, S.; Takeshita, T.; and Kern, H. 1989. Anisotropy of Vp and Vs in an amphibolite of the deeper crust and its relationship to the mineralogical microstructural and textural characteristics of the rock. Tectonophysics 157:25–38.

Skrotzki, W. 1990. Microstructure in hornblende of a mylonitic amphibolite. *In* Knipe, R. J., and Rutter, E. H., eds. Deformation mechanisms, rheology and tectonics. Geol. Soc. Lond. Spec. Publ. 54:321–325.

———. 1992. Defect structures and deformation mechanisms in naturally deformed hornblende. Phys. Status Solidi 131:605–624.

Spear, F. S., and Kimball, K. L. 1984. RECAMP: a Fortran IV program for estimating Fe super(3+) contents in amphiboles. Comp. Geosci. 10:317–325.

Speer, J. A., and Gibbs, G. V. 1976. The crystal structure of synthetic titanite, $CaTiOSiO_4$, and the domain textures of natural titanites. Am. Mineral. 61:238–247.

Stampfli, G. M., and Borel, G. D. 2002. A plate tectonic model for the Paleozoic and Mesozoic constrained by dynamic plate boundaries and restores synthetic oceanic isochrones. Earth Planet. Sci. Lett. 196:17–33.

Stünitz, H. 1993. Transition from fracturing to viscous flow in a naturally deformed metagabbro. *In* Boland, J. N., and Fitz Gerald, J. D., eds. Defects and processes in the solid state: geoscience applications: the McLaren volume (Developments in Petrology, Vol. 4). Amsterdam, Elsevier Science, p. 121–150.

Stünitz, H.; Fitz Gerald, J. D.; and Tullis, J. 2003. Dislocation generation, slip systems, and dynamic recrystallization in experimentally deformed plagioclase single crystals. Tectonophysics 372:215–233.

Tatham, D. J.; Lloyd, G. E.; Butler, R. W. H.; and Casey, M. 2008. Amphibole and lower crustal seismic properties. Earth Planet. Sci. Lett. 267:118–128.

Terry, M. P., and Heidelbach, F. 2006. Deformation-enhanced metamorphic reactions and the rheology of high-pressure shear zones, Western Gneiss Region, Norway. J. Metamorph. Geol. 24:3–18.

Uyeda, S., and Kanamori, H. 1979. Back-arc opening and the mode of subduction. J. Geophys. Res. 84:1049–1061.

Vaughan, A. P. M., and Scarrow, J. H. 2003. Ophiolite obduction pulses as a proxy indicator of superplume events. Earth Planet. Sci. Lett. 213:407–416.

Vissers, R. L. M., and Nicolas, A. 1995. Mantle and lower crust exposed in oceanic ridges and in ophiolites. Dordrecht, Kluwer Academic, 214 p.

Wenk, H.-R., ed. 2006. Neutron scattering in earth sciences. Reviews in Mineralogy and Geochemistry, Vol. 63. Chantilly, VA, Mineral. Soc. Am., 471 p.

Wenk, H.-R.; Lutterotti, L.; Grigull, S.; and Vogel, S. 2003. Texture analysis with the new HIPPO TOF diffractometer. Nucl. Instrum. Methods A515:575–588.

Wenk, H.-R.; Matthies, S.; Donovan, J.; and Chateigner, D. 1998. BEARTEX: a Windows-based program system for quantitative texture analysis. J. Appl. Cryst. 31: 262–269.

Wenk, H.-R.; Voltolini, M.; Mazurek, M.; Van Loon, L. R.; and Vinsot, A. 2008. Preferred orientations and anisotropy in shales: Callovo-Oxfordian shale (France) and Opalinus Clay (Switzerland). Clays Clay Min. 56: 285–306.

Worsley, T. R.; Nance, R. D.; and Moody, J. B. 1984. Global tectonics and eustasy for the past 2 billion years. Mar. Geol. 58:373–400.

Xie, Y.; Wenk, H.-R.; and Matthies, S. 2003. Plagioclase preferred orientation by TOF neutron diffraction and SEM-EBSD. Tectonophysics 370:269–286.

Xu, Z.; Wang, Q.; Ji, S.; Chen, J.; Zeng, L.; Yang, J.; Chen, F.; Liang F.; and Wenk, H.-R. 2006. Petrofabrics and seismic properties of garnet peridotite from the UHP Sulu terrane (China): implications for olivine deformation mechanism in a cold and dry subducting continental slab. Tectonophysics 421:111–127.

Yavuz, F. 2007. WinAmphcal: a windows program for the IMA-04 amphibole classification. Geochem. Geophys. Geosyst. 8:1–12.

Young, R. A., ed. 1993. The Rietveld method. Oxford University Press, Oxford.